Ramamoorthy Ph.D. Chemistry

Recoil Studies of Fission Products in the Fission of ^{238}U.

Ph.D.

CHEMISTRY

Anant Narayanan Ramamoorthy

RECOIL STUDIES OF FISSION PRODUCTS FORMED IN THE FISSION OF ^{238}U BY PROTONS OF ENERGIES 25-85 MeV

ABSTRACT

The recoil properties of ten fission products with masses ranging from 72 to 136 formed in the fission of ^{238}U with protons of energies 25-85 MeV have been determined radiochemically by the integral range method. From the recoil properties of the products and Monte Carlo cascade calculations, the average kinetic energy, cascade deposition energy, and anisotropy for each of the fission products has been calculated. The kinetic energy and excitation energy of the primary fragments leading to the observed fission product and the total kinetic energy and excitation energy of the primary fragment pair have also been calculated.

The results indicate that fission takes place predominantly by the compound nucleus mechanism up to an energy of 40 MeV with an increasing contribution of the direct interaction mechanism as the bombarding energy increases. The neutron deficient products are found to be formed from cascade nuclei with high-deposition energy whereas cascades with low-deposition energy lead to neutron-excessive products. The kinetic-energy deficit decreases with increasing bombarding energy. The fission products formed from the symmetric mode of fission have a larger separation distance between the charge centres of their respective primary fragments than those for the asymmetric mode of fission. No definite correlation was observed between the anisotropy and the deposition energy.

RECOIL STUDIES OF FISSION PRODUCTS FORMED IN THE FISSION OF ^{238}U BY PROTONS OF ENERGIES 25-85 MeV

by

Anant Narayanan Ramamoorthy, M.Sc. (Bombay)

A thesis submitted to the Faculty of Graduate Studies and Research in partial fulfilment of the requirements for the degree of Doctor of Philosophy

Department of Chemistry
McGill University
Montreal
Canada

June 1969

ACKNOWLEDGEMENTS

It is a great opportunity for me to express my deep gratitude and thanks to Professor Leo Yaffe for his constant encouragement, advice and guidance in this work.

I am deeply grateful to Dr. Gopal Saha for his invaluable advice and inspiration. I am ever indebted to him for all he has done for me.

I take pleasure in thanking Professor Norbert T. Porile for suggesting this experiment to me during the very early stages of this work.

My thanks are due to Drs. D.A. Marsden, M.K. Dewanjee and I. Tomita for their inspiration during the course of the experiments. The co-operation of my colleagues in this laboratory is acknowledged and greatly appreciated.

I would like to take this opportunity to thank Professor R.E. Bell, Director of the Foster Radiation Laboratory, for his permission to use the Cyclotron and Mr. R. Mills for cheerfully performing the irradiations, and also the members of the Computing Centre for executing the programmes.

My special thanks are due to Miss Ann Mylchreest for her excellent and patient typing of this thesis.

I am indebted to the National Research Council of Canada for the award of Studentships (1966-68) and to the Chemistry Department for Demonstratorships throughout the period of this work.

TABLE OF CONTENTS

TABLE OF CONTENTS

INTRODUCTION

I-1 General

Thirty years after the discovery of fission by Hahn and Strassman (1), despite a number of experimental and theoretical investigations, the fission mechanism is still an enigma today. Investigations by chemists have been made mainly on the fission products formed after evaporation of neutrons from the primary fragments produced in fission. These studies involve mainly the determination of mass-yield curves of the fission products, the dependence of yield on charge of the primary fragments, ranges and angular distribution of the fission products. From the measured values of different properties, one attempts to obtain information about the fission mechanism. Although a voluminous amount of work has been done on thermal neutron fission, studies of medium and high-energy fission are only few. Consequently more data are necessary in order to elucidate the mechanism of high-energy fission. Measurements of the recoil properties of the fission products can provide relevant information about the medium and high energy fission mechanism. The present study involves the measurements of the recoil properties of different fission products. The theoretical interpretation of the recoil properties obtained in nuclear fission is discussed briefly in the introductory part; a review of the previous work of interest is given and the purpose of the

present work is also outlined towards the end of the Chapter.

I-2 Nuclear Reactions

Two important energy-dependent mechanisms in nuclear reactions are (a) compound nucleus mechanism introduced by Bohr (2) and (b) direct interaction mechanism proposed by Serber (3). Some of the features of these two mechanisms are summarized below.

Characteristic of low energy nuclear reactions, a compound nucleus is formed through the capture of the projectile by the target nucleus. The excitation energy of this intermediate compound system equals the kinetic energy of the projectile in the centre-of-mass system plus its binding energy. The lifetime of the compound nucleus is of the order of 10^{-14} to 10^{-17} seconds, a time relatively long compared to the nuclear traversal time of a projectile. The subsequent decay of the compound nucleus is independent of the initial mode of formation and depends upon the excitation energy and composition. Decay may be by gamma emission, by evaporation of nucleons (spallation), or splitting into two nearly equal masses (fission). The angular distributions of the emitted particles or the fission fragments will be symmetric about 90° in the centre-of-mass system.

High-energy nuclear reactions can be explained by the direct interaction mechanism. The reaction at high energy is believed to proceed by a two-step process: knock-on or

cascade process followed by an evaporation process. In the fast cascade process the reaction proceeds essentially through two-body collisions between the incident particle and the individual nucleons in the target nucleus. After the initial collision both or either of the collision partners may be emitted or collide with other nucleons depending on the kinematics and energetics of the process. An intranuclear cascade is generated resulting in the emission of a few prompt nucleons with varying kinetic energy, leaving behind a residual nucleus with broad distribution of excitation energy and angular momentum. Thus this process leads to a partial transfer of energy and momentum of the incident particle to the struck nucleus. The residual nuclei will then evaporate a few more particles if energetically permissible. These residual nuclei can be treated as compound nuclei and their decay can be described accordingly.

Due to the random nature of the cascade and evaporation processes, the Monte Carlo method has been used to predict the properties of a nuclear reaction. It was Goldberger (4) who initiated the cascade calculations to find the properties of cascades using a two-dimensional model of the nucleus. Several authors (5,6,7,8,9,10) among others have adopted the same technique varying the values of nuclear parameters such as nuclear radius, nature of the potential well, and cut-off energy. The nucleus is envisaged as a degenerate Fermi gas in a square potential well with a uniform density

distribution with a sharp boundary. The most detailed calculations were made by Metropolis et al. (8,9) using a three-dimensional model for the nucleus. Though fair agreement between the calculated and experimental results has been obtained, the many instances of discrepancies at higher energies (> 50 MeV) have been attributed to the neglect of reflection and refraction of the particles at the diffuse edge of the nuclear potential well. The effects of changing from a uniform to a non-uniform radial density distribution were investigated by Bertini (11). Recent Monte Carlo calculations by Chen et al. (12) of intranuclear cascades are based on the use of a diffuse edge potential well and the inclusion of refraction and reflection of the particles at the changing potential surfaces. This calculation gives the charge, mass, excitation energy, angular and linear momenta of the residual nuclei. The Vegas calculation, as it is called, has been adopted in the present work and has been described in some detail in the discussion.

The evaporation calculations have been made on the basis of Weisskopf's statistical theory (13). Dostrovsky et al. (14,15) among others have made a very meaningful calculation of the evaporation process for many nuclei at energies up to 50 MeV. The calculation yields the charge, mass, excitation energy of the residual nuclei and also the energy spectra of the different particles.

I-3 Vector Model and Recoil Study

Momentum conservation in a nuclear reaction requires that the vector representing the direction and momentum of a recoiling nucleus must be equal to the vector sum of the momenta of the incident and emitted particles. At low projectile energies where compound nucleus formation is dominant, the total momentum of the incident particle is transferred to the struck nucleus. The compound nucleus moves along the direction of the incident projectile with an impact velocity v. In the case of direct interaction the kinematics of the nuclear reaction is more complex. The residual nucleus may move along a direction at some angle with respect to the beam direction.

The recoil products originating from the nuclear reactions will have a velocity V in the centre-of-mass system. The velocity V_L of the recoil product in the laboratory system is then given by $\vec{V}_L = \vec{v} + \vec{V}$. The vector diagrams representing the two different mechanisms are shown in Fig. 1. It is obvious from the figure that in direct interaction where $\vec{v}$ makes an angle with the incident beam axis, $\vec{v}$ can be resolved into two components, $v_{||}$ and $v_{\perp}$ which are projections of v on axes parallel and perpendicular to the incident beam respectively.

The distribution of V has often been approximated to be Gaussian. The angular distribution of V in the moving frame of the struck nucleus is symmetric about 90° to the beam axis.

Figure 1

VECTOR MODEL REPRESENTATIONS

(a) and (a'): Compound nucleus mechanism illustrating the forward, backward and perpendicular experiments.

$\vec{v}$ = impact velocity

$\vec{V}$ = evaporation or reaction velocity

$\eta = v/V$

(b) and (b'): Direct interaction mechanism, $v_{||}$ and $v_{\perp}$ are components of the knock-on velocity v, parallel and perpendicular to the beam direction; the vector V is due to the reaction velocity.

Θ and Θ_L are the recoil angles with respect to the beam direction in the system of the struck nucleus and laboratory system respectively.

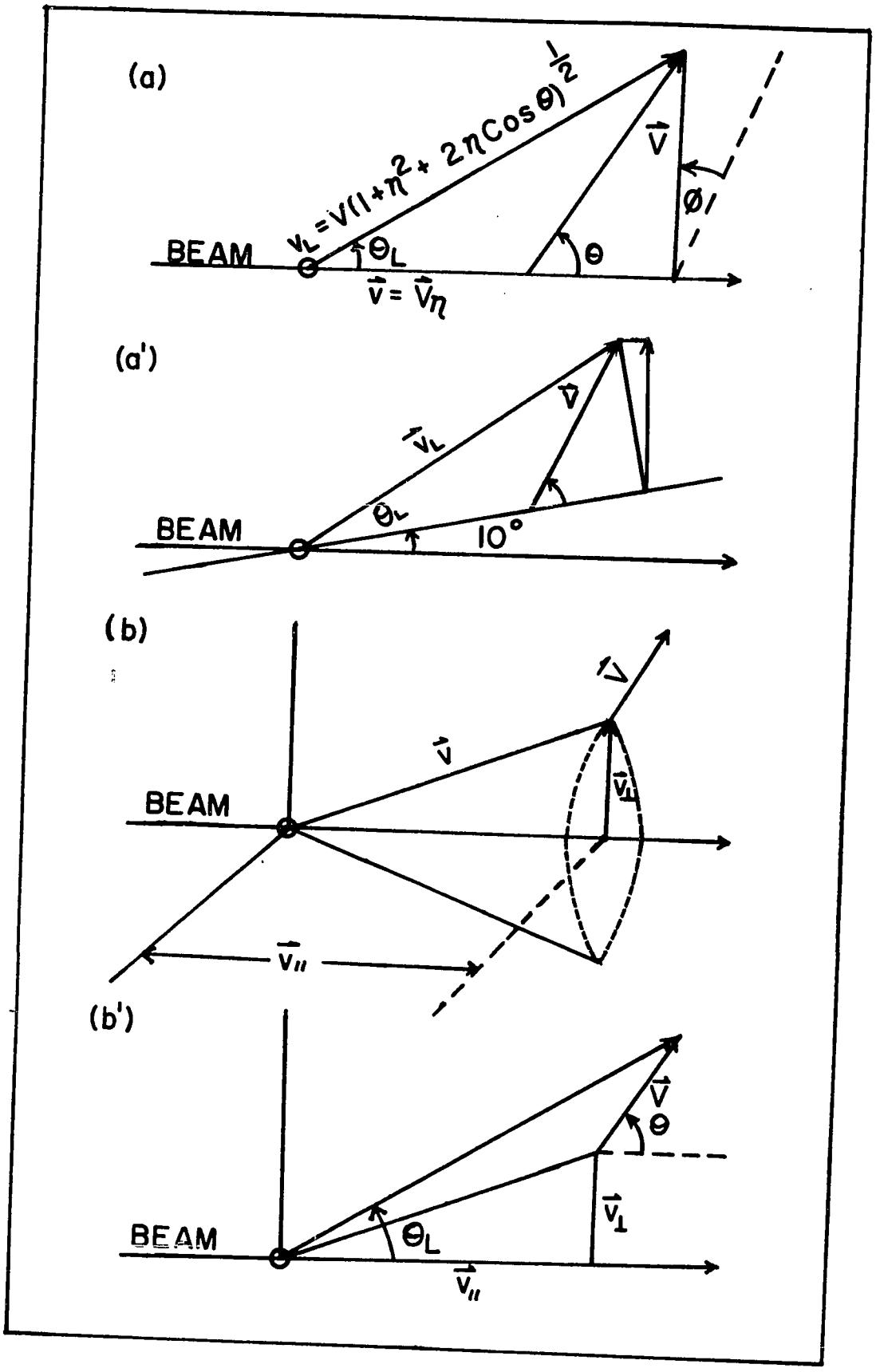
(a)
$v_L = V(1+\eta^2+2\eta\cos\theta)^{\frac{1}{2}}$
$\vec{V}$
ϕ
BEAM
θ_L
θ
$\vec{v} = \vec{V}\eta$
(a')
$\vec{V}$
$\vec{v}_L$
BEAM
θ_L
10°
(b)
$\vec{V}$
$\vec{v}$
$\vec{v}_\perp$
BEAM
$\vec{v}_\parallel$
(b')
$\vec{V}$
θ
$\vec{v}_\perp$
BEAM
θ_L
$\vec{v}_\parallel$

Ericson and Strutinski (16,17) have shown that for a large compound nucleus with spin I, the orbital angular momentum, ℓ, of the emitted particles will be preferentially parallel to the I axis and the linear momentum will be peaked in the equatorial plane. Since the compound nuclear spin I is perpendicular to the beam direction, the recoil products will be peaked in the forward and backward directions. In the light of this, and also symmetry about 90°, the angular distribution $W(\theta)$ of V is given by

$$W(\theta) = a + b \cos^2\theta$$

where b/a is called the anisotropy parameter.

In spallation reactions, the velocity V imparted to the recoils by the evaporation of nucleons is usually small compared to the impact velocity v. In fission where the fragments derive their kinetic energies mainly from the Coulomb repulsion of the two charged fragments, the velocity V of the fission fragment is much larger than the impact velocity v.

Three important recoil parameters in recoil studies are the range R (given as $R = kV^N$ where k and N are empirical constants), the velocity parameter η (given as v/V), and the anisotropy parameter b/a. The experimentally determined range R gives information about the kinetic energy of the recoil product, whereas deposition energy due to the initial interaction between the target and the projectile can be obtained from η. The b/a value yields details about the

angular distribution. Depending upon the value of η, nuclear reactions can be classified into two general categories,

(a) $\eta >> 1$. This is observed in alpha and other heavy ion-induced reactions where the impact velocity v is greater than the reaction velocity V. In this case the recoil products are all emitted in a forward cone about the beam axis in the laboratory system. The ranges of the recoil products are equal to the compound nucleus range R_{CN} corrected for the evaporation effect. The related equations have been given by Winsberg and Alexander (18,19).

(b) $\eta << 1$. Nuclear fission is a typical example of this case where v is far less than V. Because of large V and symmetry about 90°, the fission fragments will be almost equally emitted in the forward and backward directions. Winsberg (20) and Sugarman et al. (21) have independently derived equations relating the experimental projected forward, backward, and perpendicular ranges to R, $\eta_{||}$, $\eta_{\perp}$ and b/a. The detailed analysis of these equations provides information about (a) kinetic energy of a fragment (b) deposition energy of the struck nucleus and (c) the angular distribution of the fragments (see section III-2).

The recoil properties of a product formed in a nuclear reaction can be radiochemically studied by three methods: (a) 'thick target-thick catcher' or 'integral' range method (b) 'thin target-thin catcher' or 'differential' range method and (c) angular distribution method. Each experimental method

has its own merits and demerits and yields specific information about the recoil properties. These are briefly described below.

(a) 'Integral' range method: In these experiments the fractions of activities emitted in the forward, backward, and perpendicular directions are measured. The thickness of the target and the catcher foils are larger than the range of the products in the respective materials. These measured quantities are related to the average recoil properties (20, 21), as already mentioned. The recoil properties derived from these experiments, such as range (hence kinetic energy), velocity parameter η (hence deposition energy) and the anisotropy parameter b/a, are all average values. The integral range experiments facilitate the measurement of ranges of recoil products having low formation cross sections and short half-lives since only three samples corresponding to a target and two catcher foils have to be analyzed.

(b) 'Differential' range method: The distribution of recoil ranges can be obtained from these experiments. One measures the activities in a number of catchers having thicknesses much less than the range of the product. The target thickness is very small compared to the recoil range so that the recoil path remains undeviated due to the scattering in the target material. Davies and his coworkers (22,23) used thick aluminum and tungsten catcher foils and used electrostripping method to measure the activities in thin layers of

catcher foils. Katcoff et al. (24) used air as the stopping medium and collected the recoil activities on thin plastic films which were stacked at definite intervals of space. The films were analyzed for various recoil products. These experiments yield information about the distribution of ranges (hence of the recoil velocities), the range straggling, and also the mean range of the recoil products.

(c) Angular distribution method: These experiments involve the measurement of the recoil activities at different angles emitted from thin targets. These experiments provide details mainly about the symmetry about 90° in the centre-of-mass system. The laboratory angular distribution is converted to the centre-of-mass angular distribution from the kinematics of the reaction, and the anisotropy parameter b/a is then obtained as

$$b/a = \frac{\sigma(0°) - \sigma(90°)}{\sigma(90°)}$$

where $\sigma(0°)$ and $\sigma(90°)$ are the differential cross sections at 0° and 90° respectively. If direct interaction plays a role in reaction mechanism, then asymmetry of the angular distribution is encountered.

I-4 Range-Energy Relationship

The subject of mechanisms of energy loss by moving charged ions has been treated extensively by Bohr (25). The two important mechanisms by which energy loss occurs are

(a) electronic stopping (b) nuclear stopping. The charged ion moving with a velocity v loses its energy by the process of electronic stopping when $v \geq v_o$, v_o being the Bohr velocity = $e^2/\hbar^2 = 2.2 \times 10^8$ cm/sec. The moving ion transfers sufficient energy to the orbital electrons of the stopping medium by inelastic collisions, causing ionization and excitation in the stopping material. The nuclear stopping process becomes increasingly important when $v < v_o$ and the moving ion loses its energy by elastic collision with the nuclei of the stopping material. The energy transfer to the stopping nucleus may result in its ejection from its lattice if energetically permissible.

An empirical range-energy relationship generally is of the form (26,27)

$$R = k\, T^q \qquad \text{(I-1)}$$

where R and T are the range and kinetic energy of the moving ion. k and q are empirical constants whose values are determined by fitting to experimental data for the stopping of the moving ions. In general k and q are a function of the mass of the recoiling atoms and stopping material. The range energy relationship derived by Bohr (28) is of the general form

$$R = k\, M_1^{1/2} T^{1/2} Z_1^{-2/3} \qquad \text{(I-2)}$$

where the subscript refers to that of the moving ion. Similar relationship has been used by Marsh and Miskel (29) and

Brown and Oliver (30) in thermal neutron fission, who found the constant k depends on the masses of both moving ions and stopping materials.

Niday (31) has used that part of Bohr's equation (28) for the stopping power due to electronic stopping in heavy material and arrived at equation

$$R = \frac{A(V_i - V_c)}{2.411(K+4.7622K^{5/3})} \qquad (I-3)$$

Here R is the range in mg/cm^2, V_i is the initial velocity in units of 10^8 cm/sec, A is the mass number of the moving ion, V_c is the critical velocity of the fragment below which the scattering may be assumed to be of the hard-core type. It is evaluated by equating the 'collision diameter' $d(=2Z_1Z_2e^2/\mu V_c^2)$ with the screening radius $a[a_o(Z_1^{2/3}+Z_2^{2/3})^{1/2}]$, where μ is the reduced mass of the system, a_o is the first Bohr radius of the hydrogen atom, Z_1 and Z_2 are the charges of the fragments and the stopping material. K is the effective charge function and is a difficult parameter to estimate. Since a moving fragment will continually pick up and lose electrons when passing through matter, Niday took into account the charge dependence by using $K = k_1 Z_p^{1/3}$ where k_1 is an adjustable parameter and Z_p is the most probable charge for the chain mass of the fragment. He used initial energies from Stein's measurements (32) and the assumption that 1.25 neutrons were emitted from each fragment (32). With aluminum catchers he found $k_1 = 1.077$ to provide excellent agreement between calcu-

lated and experimental ranges in the mass region 89-156. Lassen (33) showed that the effective charge function K has a weaker charge dependence for light fission fragments than for heavier fragments. It appears that additional parameters are needed in equation (I-3) to describe the range in the light mass range.

The recent theory of Lindhard et al. (34) provides a universal range-energy relationship for all recoiling atoms in all stopping materials. They are briefly summarized as follows.

$$\rho(\varepsilon) = (2/k)\varepsilon^{1/2} - \Delta(k,\varepsilon) \qquad \text{(I-4)}$$

where $\rho(\varepsilon)$ and ε are dimensionless measures of the range and the kinetic energy respectively, k is a parameter depending upon M_1, M_s, Z_1 and Z_s where subscripts 1 and s refer to that of the moving charged ion and the stopping material respectively; $\Delta(k,\varepsilon)$ is a term responsible for the nuclear stopping phenomenon. These quantities are explicitly given by

$$\rho(\varepsilon) = 4\pi a^2 NRM_1M_s(M_1+M_s)^{-2} \qquad \text{(I-5)}$$

$$\varepsilon = aTM_s[Z_1Z_2e^2(M_1+M_s)]^{-1} \qquad \text{(I-6)}$$

$$k = 0.0793\xi Z_1^{1/2}Z_s^{1/2}(M_1+M_s)^{3/2}Z_o^{-3/4}M_1^{-3/2}M_s^{-1/2} \qquad \text{(I-7)}$$

$$\Delta(k,\varepsilon) = \int_0^{\varepsilon} (d\varepsilon/d\rho)_n (d\varepsilon/d\rho)^{-1} (d\varepsilon/d\rho)_e^{-1} d\varepsilon \qquad \text{(I-8)}$$

Here a is $0.8853\ a_o Z_o^{-1/2}$ where a_o is the Bohr radius in the hydrogen atom and $Z_o = Z_1^{2/3} + Z_s^{2/3}$, N is the number of stopping atoms per cubic centimeter; R is the range in centimeters, and ξ is approximately given by $Z_1^{1/6}$. In equation (I-8) subscripts n and e refer to the rate of energy loss due to nuclear stopping and electronic stopping processes respectively. The values of $\Delta(k,\varepsilon)$ are obtained by interpolation of graphs given by Lindhard et al. (34).

Noshkin and Sugihara (35) have obtained a simplified version of the range-energy relationship of Lindhard et al. The term representing the nuclear stopping mechanism of energy loss in equation (I-4) is cumbersome to evaluate. Briefly the procedure of utilizing this relationship is to calculate ρ from the experimentally measured R using the equation (I-5). Then for an estimated value of ε, $\Delta(k,\varepsilon)$ and ε are determined. Successive improvements are made in the value of ε until a constant value of ε is obtained. To circumvent this procedure Noshkin and Sugihara (35) have obtained the following relationship:

$$\rho(\varepsilon) = (c/k)\varepsilon^{1/2} \qquad \text{(I-9)}$$

where c is an empirical constant. In order to evaluate c, ranges of fragments in thermal neutron fission of ^{235}U, measured by various authors for several stopping materials (Al (30,31,36,37,38,39,40), Zr (43), Au (36) and U (31)) were converted to $\rho(\varepsilon)$ and the kinetic energies ε by use of the equations of Lindhard et al. (34). These values of $\rho(\varepsilon)$ and ε

could be correlated by equation (I-9) with a value of 1.30 for c. Hogan and Sugarman (41) obtained a value of c = 1.312 from a least squares fit of the equation to Niday's (31) range-energy data of only heavy fission products stopped in uranium.

Sugarman et al. (21) used the empirical range-energy relationship similar to the equation (I-1) with the assumption that the empirical constants depend upon the masses of the recoiling fragments. The empirical constants k and q were estimated from the analysis of the range-energy data for heavy ions and for fission fragments in thermal neutron fission. The dependence of range on the nuclear charge of the fragment was ignored.

I-5 Previous Work of Interest

Recoil studies have been reviewed from time to time, by Walton (42), Harvey (43), and recently by Alexander (44). From these reviews one obtains various information about reaction mechanisms in different recoil experiments. Since the present work involves the measurement of the recoil ranges of fission products from ^{238}U fission by the integral range method, a brief review of the pertinent recoil studies is outlined below.

Porile and Sugarman (45) investigated the recoil properties of fission fragments formed in 450-MeV proton fission of bismuth and tantalum using radiochemical techniques. The total average kinetic energy released in fission was found to

be 111 MeV for bismuth and 96 MeV for tantalum. A Monte Carlo calculation for the cascades from Metropolis et al. (8,9), gave the average deposition energy in the fission of bismuth and tantalum to be 160 MeV and 190 MeV, respectively.

Niday (31) studied the ranges of 28 fission products from thermal neutron fission of ^{235}U using the integral-range method. The average total kinetic energy was found to be 30 MeV less for the events in symmetric fission than those in asymmetric fission. The observed low ranges of shielded ^{136}Cs and ^{86}Rb nuclides had been attributed to the combined effect of higher distortion energy with lower coulomb repulsion, and higher total beta decay energy in addition to the effect of the increased nuclear charge of the shielded nuclides. Brown and Oliver (30) measured the ranges of ^{136}Cs, ^{137}Cs, and ^{140}Ba in thermal neutron fission of ^{235}U by the differential-range method and found that the total kinetic energy in the fission mode leading to ^{136}Cs is about 21 MeV less than that in the mode leading to ^{137}Cs and ^{140}Ba. Differential ranges have been measured for 19 fission products from the spontaneous fission of ^{252}Cf by Marsh and Miskel (29). In the plot of range versus mass number, a dip in the vicinity of symmetric fission was not observed, in contradiction to the kinetic energy data obtained from time-of-flight measurements of Stein and Whetstone (46) but in agreement with the data of Milton and Fraser (47).

Alexander et al. (27,36,48) measured the ranges and kinetic energies of several fission products produced from 0.72,

3.0, and 6.2-GeV proton irradiation of ^{238}U using the Monte Carlo cascade calculation of Metropolis et al. (8,9) and the relationship between the deposition energy and forward momentum of the cascade given by Porile (49), they also calculated the average deposition energy for processes leading to each fission product. They concluded from their studies that the observed fission products at 0.72 GeV and the neutron-rich products at 3 and 6.2 GeV are formed from binary fission and the deposition energies deduced are of the same order as the calculated deposition energy for all reactions. At 3.0 and 6.2 GeV, the neutron-deficient products were thought to be produced from a fast break-up process. Aras et al. (50) made measurements of ranges of several fission products from fission of ^{235}U with thermal neutrons. A total kinetic energy deficit of 21 MeV was observed in the region of symmetric fission agreeing with that reported by Alexander et al. (27) and Niday (31) but at variance with those obtained by Milton and Fraser (47) from the time-of-flight measurements and by Gibson et al. (51) from the semiconductor detector work. They suggested that the values from the range data are more reliable than those obtained from direct instrumental experiments because of the difficulties of mass dispersion and low number of events in the symmetric region encountered in the latter method. Mukerji and Yaffe (52) have measured the ranges of ^{140}Ba in proton-induced fission of ^{238}U, by stripping thin layers of aluminum from forward and backward catcher foils.

They reported full momentum transfer at 15, 30 and 60-MeV irradiations. The range-velocity relation of Bohr had been modified to include the fact that the "effective charge" can be expressed as a function of the charge and mass of the medium penetrated.

Recoil properties of fission fragments in 150-MeV proton fission of ^{238}U had been studied by Noshkin and Sugihara (35,53). Using a simplified version of the theoretical range-energy equation proposed by Lindhard et al. (34), they observed that the total energy release was essentially the same for symmetric and asymmetric fission and the average value was found to be 161 MeV. Using the two-step model for the nuclear reaction they also contended that the data were consistent with fission occurring according to the unchanged charge distribution hypothesis. The average deposition energy was found to be 68 MeV compared to 87 MeV as given by the Monte Carlo calculations of Metropolis et al. (8,9). Furthermore, the neutron-deficient products were found to be formed from high-deposition events and the neutron-rich products from low-deposition events.

Sugarman et al. (21) studied the recoil behaviour of a number of fission products formed from 450-MeV proton fission of ^{238}U. The average total kinetic energy was reported to be 163 MeV. The fission fragments formed from events of low-deposition energy were found to have a preferential perpendicular emission and those formed from events of

high-deposition energy had a preferential forward-backward emission. The momentum deposition energy relation obtained from the Monte Carlo calculations led to an average cascade deposition energy of 123 MeV for the overall fission process, a value lower than 147 MeV, calculated for all cascades.

Crespo et al. (54) in their recoil studies in the fission of ^{238}U by 2.2 GeV protons, found that the neutron-deficient isotopes have broader momentum distributions and more forward peaked angular distributions than do the neutron excess products. They explained qualitatively that the negative value of b/a is a feature of low-deposition energy and positive b/a is that of high-deposition energy. Saha and Yaffe (55) measured the recoil properties of ^{66}Ni, ^{67}Cu, and ^{72}Zn in ^{238}U fission by 40-85-MeV protons. The fission fragments at these bombardment energies were found to arise mainly from the compound nucleus mechanism. The average total kinetic energy released in the fission process was calculated to be 163 MeV. Hogan and Sugarman (41) studied the recoil behaviour of 20 heavy nuclides in 440-MeV fission of ^{238}U. In the isobaric fission products, the kinetic energy decreased linearly with increasing charge and the cascade deposition energy increased linearly with increasing charge. The observed change in anisotropy of the angular distributions of isobaric fission products formed from events of high deposition energy and of low deposition energy, was explained by use of the angular momentum data of the cascade nucleus and the

theoretical interpretation applied to fission induced by protons of less than 40 MeV. They have also explained the decrease in kinetic energy for a more neutron-deficient fission product, in terms of the deformation of the fissioning nucleus and the energetics of the fission process leading to a neutron deficient product.

I-6 Purpose of Present Work

The present work involves a study of 10 recoil products formed from the fission of ^{238}U induced by protons of 25, 40, 55, 70, and 85-MeV energies. Information regarding recoil behaviour of fission products formed in this energy region is lacking. The fission products chosen cover the region in the Yield-Mass curve from light to heavy masses thereby facilitating the comparison of the recoil properties of fission products formed in symmetric and asymmetric region. The choice of shielded and cumulative isotopes helps to explain some of the mechanisms of the fission. The following presentation, however, obviously does not pretend to be an exhaustive study; it will give some information about the kinematics and fission mechanisms in this energy region.

II. EXPERIMENTAL PROCEDURES

II-1 General

The experimental procedure, adopted here for the measurement of recoil properties of some of the fission products, is similar to that used by Sugarman and coworkers (21,45,56,57), referred to as "thick target-thick catcher" experiments. "Thick target-thick catcher" refers to the thickness relative to the ranges of the fission products which vary from 7 to 13 mg/cm^2 in uranium, 3 to 6 mg/cm^2 in aluminum for the nuclides studied in the present work.

II-2 Target Assembly

The target assemblies for two types of irradiations are shown in Fig. 2. In one, the target assembly is normal to the proton beam and the products recoiling from the target (T) in forward and backward directions to the beam are collected in the forward (F) and backward (B) catchers. This is called a forward-backward experiment (Fig. 2(a)). For the other type of experiment, designated as a perpendicular experiment, the perpendicular aspect of the target assembly is approximated by a 10° tilt relative to the proton beam (Fig. 2(b)) and the recoils are collected in the up (U) and down (D) catchers. In these experiments, the activities in the U and D catchers are nearly the same.

The uranium target was .003" thick and of natural

FIGURE 2

THICK-TARGET ASSEMBLIES SHOWING THE TWO ORIENTATIONS USED FOR STUDYING THE RECOIL BEHAVIOUR

(a) Forward-backward and (b) Perpendicular.

G - guard foil; B - backward catcher foil;

T - target; F - forward catcher foil;

A - activation foil.

(c) Target assembly clamped to the target holder.

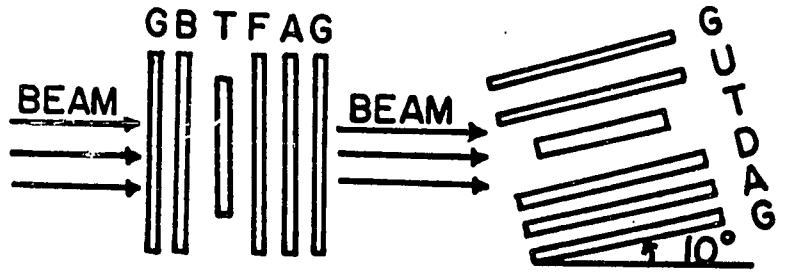
GB T F AG
BEAM
BEAM
G
U
T
D
A
G
10°

(a) (b)

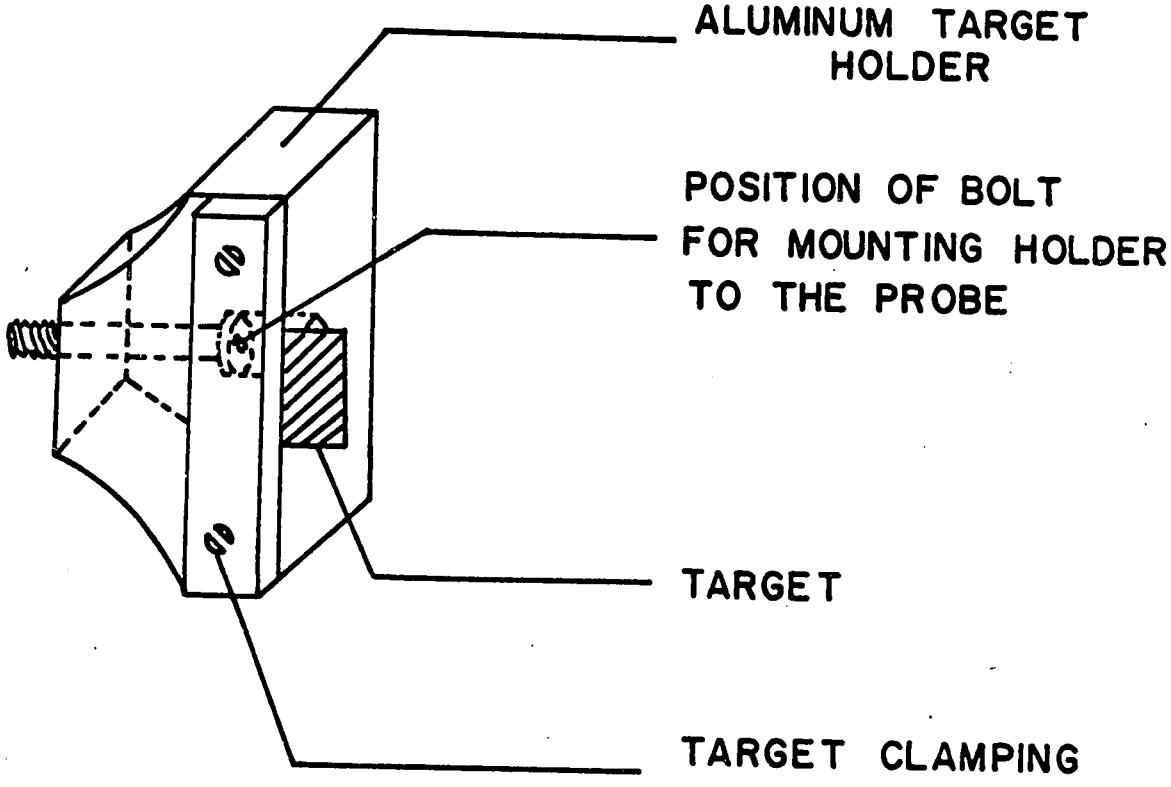
ALUMINUM TARGET HOLDER
POSITION OF BOLT FOR MOUNTING HOLDER TO THE PROBE
TARGET
TARGET CLAMPING SCREWS

(c)

isotopic composition. Freshly-cleaned uranium foils develop a thin layer of relatively loose uranium oxide film. The aluminum catcher foils, in close contact with the target foil, after irradiation contain only about 1.5 to 3% of the total target activity. They may, however, contain spurious activity if physical transfer of the oxide from the target occurs unless special precaution was taken. The following procedure was used in order to use the uranium foils of more or less the same thickness and also avoid further oxidation.

Several uranium foils of 2 cm x 1 cm size were cleaned in concentrated nitric acid, each for 15 seconds and washed with water. They were immersed, one by one, in a beaker containing 25 ml of water, 15 ml of saturated ammonium oxalate solution and 12 mg of uranyl nitrate, maintained at 80°C (58). A platinum helix attached to the end of a glass rod served both as an anode and a stirrer. A 12-volt power supply was used. The cleaned uranium foil was the cathode. A rheostat was inserted into the assembly in order to have a current density of about 120 ma/cm^2 at the cathode. The two sides were directed towards the stirring anode for 5 seconds each. The deposited layer was found to adhere strongly to the foil and could not be removed by rubbing. The thickness of the deposit was estimated to be less than 10 micrograms/cm^2 (58). The foil resisted further oxidation and retained its weight and colour for periods of several months. The thickness of the deposit is negligible compared to the ranges of the fission products studied in the present work.

Each of the foils was weighed accurately and its area measured using a travelling microscope. An average value of 145.3 mg/cm^2 was obtained from six measurements and it did not vary from any one value by more than 2.5%.

The target foil was sandwiched between two aluminum catcher foils of thickness 9.2 mg/cm^2 which overlapped the target on three sides by 2 mm, the fourth side to be fastened in the target holder. The purity of the catcher foil was checked by using an activation foil (Fig. 2) of the same aluminum as used for the catcher and analyzing for different products of interest. The correction for activation was found to be negligible at all energies. The complete set of target-catchers was enveloped by a wrapping foil of aluminum of the same quality as the catcher foil. The target assembly was fastened to the target holder which in turn was attached to the end of the water-cooled Cyclotron probe. The maximum exposure of the target to the proton beam was ensured by positioning the target properly in the holder according to the energy variation of the vertical oscillation of the proton beam. The target assembly was then placed at a radial distance corresponding to the desired bombarding energy. The radial distance was obtained from the radius-versus-energy curve supplied by the Cyclotron group.

II-3 Irradiation

All irradiations were performed in the internal

circulating proton beam of the McGill Synchrocyclotron. Bombardments were made at 25, 40, 55, 70 and 85 MeV. The duration of irradiations varied from 15 minutes to 1 hour depending upon the formation cross section of the fission product, bombarding energy, and the beam intensity which varied from 0.5 to 1 microampere.

II-4 Chemical Separation

After irradiation, the target and the catcher foils were dismantled noting carefully which were the forward and backward foils. In forward and backward experiments, there are three samples, forward, backward and target, for radioassay. In perpendicular experiments the two catcher foils were combined to give one sample and thus there were only two samples including the target to assay. The foils were transferred into respective centrifuge tubes which already contained the requisite amount of carriers and hold-back carriers, if necessary, and which had previously been evaporated to dryness under an infra-red lamp. Wherever it was possible, radiochemical analyses were performed for more than one element in a single irradiation. Since the target was, in general, about 50 times more active than either catcher foil, the carriers added to the target sample was about 10 to 15 times that added to either catcher foil sample. After dissolution of the target foil and proper exchange of the carrier and radioactive fission product, suitable aliquots

of the target solution were taken for the radioassay in such a way as to get samples of roughly equal weight of the carrier and activity. Since only relative activities are needed, this avoided any necessity for corrections due to self-absorption, dead time and greatly diminished the hazard of cross contamination. The glassware used for target analysis was isolated from that used for the catcher foils. The chemical procedures adopted here are mainly based on those reported in the Nuclear Science Series for gallium (59), bromine (60,61), yttrium (62), silver (63) and cesium (64,65).

Cesium:

The isotope of interest was ^{136}Cs, which has a half-life of 13 days. In the same irradiation, the samples were also analyzed for ^{111}Ag (7.5 day half-life). Since ^{136}Cs is shielded and relatively long-lived, a quick separation from other fission products is not necessary. ^{111}Ag is cumulatively measured and the irradiated foils were processed after about 48 hours to ensure complete decay of the precursors.

The target was dissolved in 10 ml of conc. nitric acid, in the presence of 150 mg each of Cs, Rb, Ag, and Pd carriers. The solution was made up to a suitable volume in the same tube and 1/15 volume of the solution was taken for the analysis of the target sample. The aluminum catcher foils were dissolved in about 7 to 8 ml of dilute nitric acid (~1N), a few drops of 10% H_2O_2 and about 25 mg mercuric nitrate in the presence of 10 mg each of Cs, Rb, Ag, and Pd carriers.

Usually a gentle heating initiated the process of dissolution.

In each sample, chloride precipitation was performed with 1 ml of 6N HCl. After proper digestion of the precipitate in the solution, the silver chloride precipitate was preserved for the isolation and purification of ^{111}Ag which is described later. The supernatant containing Cs and Rb among other elements, was evaporated to dryness. It was converted to nitrate by repeated evaporations with small volumes of conc. HNO_3. To each of the samples 5 ml of 70% perchloric acid was added and boiled gently until dense fumes of perchloric acid appeared. The solutions were then cooled in ice and to each, 15 ml of absolute alcohol was added. The precipitates of Cs and Rb were centrifuged and washed twice with 5 ml of absolute alcohol. The precipitate was dissolved in 5 ml of water and a ferric hydroxide scavenging with 5 mg of Fe^{3+} as nitrate was performed using a minimum quantity of 6N ammonium hydroxide. The samples were centrifuged and ferric hydroxide was again precipitated from the supernatant and filtered. From the filtrate, free ammonia was driven off by gentle heating with a minimum quantity of 2N NaOH. When there was no more ammonia evolving, as verified by using litmus paper, the perchlorate precipitation was performed as before, followed by washing with absolute alcohol. The perchlorates were dissolved in 3 ml of water, acidified with 3 drops of glacial acetic acid, and 1 ml of HI-BiI_3 reagent (10 gm of BiI_3 dissolved in 50 ml of 55% HI) was added to precipi-

tate cesium as $Cs_3Bi_2I_9$, leaving rubidium in solution. The solution was cooled in ice for several minutes. After centrifugation, the precipitate was washed with 7 ml of cold water and 1 ml of 2N HCl. After decomposition of the precipitate with 6 drops of conc. HCl, $Cs_3Bi_2I_9$ precipitation was repeated with 5 mg of Rb hold-back carrier. The precipitate was washed as before and decomposed with 6 drops of conc. HCl. Bi was removed as hydroxide with a minimum quantity of 2N NaOH. Final precipitation of cesium perchlorate was performed followed by washing with ethanol. The precipitate was dispersed in 10 ml of absolute ethanol and filtered through a Whatmann #40 paper disc of 2.4 cm diameter which had previously been weighed after proper conditioning. The perchlorate precipitate was uniformly spread, by filtering very gently. The precipitate was dried at 110°C for 15 minutes in an oven, cooled and the weight determined accurately. The samples thus obtained were mounted on a cardboard and covered with Mylar film for beta measurements.

Silver:

The isotopes of interest are ^{111}Ag, ^{112}Ag, and ^{113}Ag. The decay chains of ^{112}Ag and ^{113}Ag are

Short half-life $\xrightarrow{\beta^-}$ ^{112}Pd (21.0 h) $\xrightarrow{\beta^-}$ ^{112}Ag (3.2 h) $\xrightarrow{\beta^-}$ ^{112}Cd (stable)

Short half-life $\xrightarrow{\beta^-}$ ^{113}Pd (1.5 m) $\xrightarrow{\beta^-}$ ^{113}Ag (5.3 h) $\xrightarrow{\beta^-}$ ^{113}Cd (stable)

Being semi-shielded, ^{112}Ag should be separated quickly from the precursor ^{112}Pd in such a time that the contribution from the parent can be neglected. The analysis for the cumulatively-formed isotope of ^{113}Ag was performed in the same irradiation. The irradiation for the analyses of ^{112}Ag and ^{113}Ag usually lasted for about 20 minutes and it took another 10 minutes for the initial chloride separation of silver from palladium. A period of 10 minutes was sufficient for the decay of most of the ^{113}Pd (half-life = 1.5 min.) to ^{113}Ag. As mentioned earlier, a single irradiation yielded samples of both ^{136}Cs and ^{111}Ag.

The irradiated foils for the analyses of ^{112}Ag and ^{113}Ag, were dissolved quickly adopting the same procedure used for the analysis of Cs. A quick silver chloride precipitation was done, using 10 mg of Pd hold-back carrier. The precipitate of AgCl was dissolved in 2 ml of 6N NH_4OH and a ferric hydroxide scavenging was performed using 5 mg of Fe^{3+} as nitrate. The precipitate was discarded after centrifugation and the supernatant ammoniacal solution was saturated with hydrogen sulphide gas to remove silver as Ag_2S. After washing with ammoniacal water, the precipitate was dissolved in conc. HNO_3. A hydroxide scavenging with Fe^{3+} followed by sulphide precipitation was repeated and a final scavenging by ferric hydroxide was followed by filtration through Whatmann #40 filter paper. To this ammoniacal solution 5 drops of conc. HCl were added. The solution was acidified with nitric acid until a permanent chloride precipitate appeared. Before the chloride

precipitate coagulated, it was centrifuged and washed with water. With the aid of the fire-polished end of a glass rod the precipitate was made into a fine paste, before being transferred to a previously-weighed Whatmann #40 filter paper disc. The samples were prepared for measurement of beta activity, as described earlier.

Yttrium:

The isotopes of interest of yttrium are ^{90}Y and ^{93}Y and their decay chains are

$$^{90}Sr \underset{(28\ y)}{\xrightarrow{\beta^-}} {}^{90}Y \underset{(64.2\ h)}{\longrightarrow} {}^{90}Zr \text{ (stable)}$$

$$\text{Short half-life} \longrightarrow {}^{93}Sr \underset{(8\ m)}{\xrightarrow{\beta^-}} {}^{93}Y \underset{(10.1\ h)}{\xrightarrow{\beta^-}} {}^{93}Zr \ (10^5\ y)$$

Since in the same irradiation the foils were analyzed for the semi-shielded isotope ^{90}Y and cumulative ^{93}Y, the irradiated samples were cooled for 2 hours to permit complete decay of ^{93}Sr ($T_{1/2}$ = 8 min.) to ^{93}Y, neglecting the contribution of ^{90}Sr to ^{90}Y.

The target foil was dissolved in 5 ml conc. HCl and a few drops of conc. HNO_3 in the presence of 70 mg of yttrium carrier and 100 mg each of zirconium and strontium hold-back carriers. The catcher foils were dissolved in the same acids in the presence of 7 mg of yttrium and 10 mg each of strontium and zirconium carriers. After complete dissolution suitable aliquots of the target solution were taken for analysis.

Yttrium was precipitated as $Y(OH)_3$ by adding an excess of conc. NH_4OH. The hydroxide precipitate was centrifuged, dissolved in dilute HCl, and hydroxide precipitation was repeated with strontium hold-back carrier. The $Y(OH)_3$ precipitate was dissolved in 2 ml of conc. HNO_3 and transferred to a teflon tube. The solution was diluted to about 10 ml with water and YF_3 was precipitated with 2 ml of conc. HF. The precipitate was washed with 10 ml of 5N HF, dissolved in a mixture of 2 ml of saturated boric acid and 3 ml of nitric acid and the fluoride precipitation of yttrium was repeated with 10 mg of zirconium hold-back carrier. The fluoride precipitate was again dissolved in H_3BO_3-HNO_3 mixture and precipitation of hydroxide with 6N NH_4OH was made.

$Y(OH)_3$ was dissolved in about 5 ml of conc. HNO_3 and transferred to a separatory funnel containing 10 ml of tributyl phosphate (40/60 V/V in petroleum ether) which was previously equilibrated with conc. HNO_3. The centrifuge tube was washed with another 20 ml of conc. HNO_3 and transferred to the funnel and the mixture shaken. The organic phase containing yttrium was scrubbed twice with 25 ml of conc. HNO_3 and then yttrium was back-extracted twice with 25 ml portions of water. A hydroxide precipitation, followed by a fluoride precipitation with zirconium hold-back carrier and a second solvent extraction cycle resulted in obtaining yttrium in 20 ml of aqueous solution. $Y(OH)_3$ was precipitated,

washed with water, dissolved in 2 ml of 6N HCl and made up to about 10 ml, with water. The solution was warmed and 15 ml of saturated ammonium oxalate was added to precipitate yttrium oxalate. The oxalate precipitate was filtered on to a 2.4 cm diameter Whatmann #42 filter paper disc through a Hirsh funnel-filter set-up, washed with water and ignited at 850°-900°C for about 50 minutes in a Coors OO porcelain crucible. The Y_2O_3 was cooled and powdered with a fire-polished glass rod. The powdered yttrium oxide was then transferred with methanol on to a weighed, Whatmann #40 paper disc. Y_2O_3 was then dried at 110° for 15 minutes, cooled and weighed and mounted on a cardboard mount and covered with Mylar for beta measurement.

Bromine:

The isotopes of interest in the present work are ^{82}Br (shielded) and ^{83}Br (cumulative). The decay chain of ^{83}Br is

$$^{83}Se \underset{(25\ m)}{\xrightarrow{\beta^-}} {}^{83}Br \underset{(2.4\ h)}{\xrightarrow{\beta^-}} {}^{83}Kr \text{ (stable)}$$

The target and catcher foils were placed in their respective tubes containing suitable amount of bromide and iodide carriers. The target uranium was dissolved in conc. HCl and the catcher aluminum foils were dissolved in dilute HCl (4N). A drop of nitric acid cleared the solution. The samples were neutralized gradually and finally made alkaline with 6N NaOH and 12N NaOH so that the total volume was about 10 ml of 4N NaOH. One ml of 5% NaClO was added and digested

slowly. The solution was acidified slowly with conc. HNO_3 until it was acidic and transferred to a separatory funnel containing 10 ml of CCl_4. Three ml of 1M $NH_2OH \cdot HCl$ was added and the iodine removed into the organic phase which was discarded. To the aqueous bromide layer a few drops of 1M $KMnO_4$ were added until there was a permanent colour in the aqueous layer due to the free permanganate. The free bromine was extracted into a fresh 10 ml of CCl_4 layer discarding the aqueous layer. Bromine was reduced to bromide with 1 ml of 1M $NH_2OH \cdot HCl$ and the bromide was extracted into the aqueous layer. Two more oxidation-reduction cycles, oxidation with $KMnO_4$ in nitric acid medium and reduction with 1M $NaHSO_3$, were performed to complete the oxidation-reduction cycles.

To the bromide aqueous solution, 1 ml of 6M HNO_3 was added and boiled to remove any free SO_2 gas. Then 2 ml of 0.1M $AgNO_3$ was added to precipitate AgBr and samples were made for beta counting as before.

Gallium:

The isotopes of ^{73}Ga (cumulative) and ^{72}Ga (semi-shielded) were measured and their decay chains are

Short half-life $\xrightarrow{\beta^-}$ ^{73}Ga (4.8 h) $\xrightarrow{\beta^-}$ ^{73}Ge (stable)

^{72}Zn (46.5 h) $\xrightarrow{\beta^-}$ ^{72}Ga (14.1 h) $\xrightarrow{\beta^-}$ ^{72}Ge (stable)

A quick separation of ^{72}Ga was necessary to minimize the contribution from ^{72}Zn. The target and the catcher foils were dissolved in 2 ml of conc. HCl and a few drops of conc. HNO_3, in 40 ml centrifuge tubes containing Ga and Zn carriers, the latter being the hold-back carriers. A quick separation of Ga from Zn was performed by the solvent extraction of Ga into 10 ml of isopropyl ether, pre-equilibrated with 6N HCl, from a 6N HCl solution of the foils. The organic phase was scrubbed with two 10 ml portions of 6N HCl and Ga was back-extracted into 10 ml of water. The aqueous solution containing Ga was scavenged with copper, cadmium, and molybdenum sulphides. The supernatant solution of gallium was made alkaline with 12N NaOH. The alkaline solution was scavenged with $Fe(OH)_3$ and Ba-Sr carbonates. The pH of the supernatant was gradually decreased to yield a precipitate of $Ga(OH)_3$. The precipitate was dissolved in dilute HCl and sulphide, hydroxide-carbonate, scavengings were repeated. A second ether extraction was performed and gallium was precipitated as gallium oxinate with 8-hydroxy quinoline at pH 6. The precipitate was washed with water, dried at 110°, weighed and mounted as before for measurement of β-activity.

II-5 Proportional Beta Counters

The radioactivity of the decaying nuclides, studied in the present work, was measured by the detection of the emitted beta rays. As we are interested in the relative

yields of the activities in the target and the catcher foils, the samples were mounted in identical fashion and measured in the same geometrical arrangement to avoid any efficiency corrections. Two types of beta counters were used to measure the beta activity of the different nuclides. The characteristic features of the counters are tabulated in Table I.

TABLE I

Characteristics	Baird Atomic model- 135	Sharp model LB-100
Operative voltage (V)	2250	2100
Plateau length (ΔV)	$\sim$ 400	$\sim$ 200
Detector diameter (in.)	1.5	2.0
Window thickness ($\mu g/cm^2$)	$\sim$ 900	$\sim$ 800
Resolving time (μs)	$\sim$ 25	$\sim$ 300
Source mount	Cardboard & stainless steel	Cardboard & stainless steel
Anode wire	tungsten	stainless steel
Background rate (cpm)	12 $\pm$ 1	1.1 $\pm$ 0.2
Counter gas	90% argon 10% methane	90% argon 10% methane

The detector in the beta counter is operated in the proportional region in which the pulse height at a particular detector voltage is proportional to the initial ionization caused by the incident particle. The upper and lower limits of sensitivity are set by the dead-time and the activity level of the environment, including the activity of the materials of construction of the detector.

For high-level beta activity measurements, an end-window gas flow proportional counter (Baird Atomic model-135) was used. It is a compact unit consisting of a Scaler, a Timer, a High-Voltage Power Supply, and a Low-Voltage Power supply. The Scaler contains five glow-type decatron register tubes, and the Timer is provided with four tubes. The detector is coupled to the Scaler through a pre-amplifier (Model-225). For every input pulse, one count is recorded. The maximum recording capacity is 10^5 counts. The detector was operated at 2250 volts with the discriminator bias set at 2 volts. The background varied from 11 to 13 counts per minute. The stability of the unit was regularly checked with a standard ^{36}Cl source. Two counters of the same type were used for measuring the beta activities of the samples, which in many cases were alternated between these two counters to get duplicate counting rates.

For low-level activity measurements, a low-level beta counter (Low Beta, series LB-100, Sharp Lab., La Jolla, California) was used. The detector chamber in this counting

system is heavily shielded with high-purity aged lead and copper to minimize the natural background. It operated in anti-coincidence with the environment background and cosmic rays by means of a guard detector. Samples for this counter were prepared on stainless steel planchets which had a low background of 0.8-1.2 counts per minute. The dead-time was 300 microseconds. The stability of the instrument was regularly checked with the standard ^{36}Cl source.

All the detectors used for beta radiation measurements were the gas-flow type and a mixture of 90% argon and 10% methane was used as the counting gas.

II-6 Measurement of Beta Radiations

The decay characteristics of different nuclides were taken from "Table of Isotopes" edited by Lederer et al. (66). These properties and their detection techniques are summarized in Table II.

The fission products studied in this work are present in the following mass chains:

(i) ^{136}Cs (13 day) $\xrightarrow{\beta^-}$ ^{136}Ba (stable)

(ii) short $\xrightarrow{\beta^-}$ ^{112}Pd (21.0 h) $\xrightarrow{\beta^-}$ ^{112}Ag (3.2 h) $\xrightarrow{\beta^-}$ ^{112}Cd (stable)

(iii) short $\xrightarrow{\beta^-}$ $^{111}Pd^m$ (5.5 h) $\xrightarrow{25\%}$ ^{111}Ag (7.5 day)

$^{111}Pd^m$ $\downarrow$ 75%

$^{111}Pd^g$ (22 m) $\nearrow$

$\xrightarrow{\beta^-}$ ^{111}Cd (stable)

TABLE II

Radiation Properties of Measured Nuclides

Nuclide	Half-life	Radiation* Energy (MeV)	Branch Abundance (%)
^{136}Cs	13 d	0.66	7
		0.34	93
^{113}Ag	5.3 h	2.0	100
^{112}Ag	3.2 h	3.94	54
		3.35	22
		1.96	10
		(others)	4
^{111}Ag	7.5 d	1.04	91
		0.80	1
		0.70	8
^{93}Y	10.2 h	2.89	90
		(others)	10
^{90}Y	64.0 h	2.27	100
^{83}Br	2.41 h	0.92	98.6
		0.39	1.4
^{82}Br	35.34 h	0.44	100
^{73}Ga	4.9 h	1.19	95
		0.4	5
^{72}Ga	14.1 h	3.17	8
		2.53	9
		1.51	10
		0.96	31
		0.64	42

* All radiation energies are those of β rays.

(iv) short $\xrightarrow{\beta^-}$ ^{113}Ag $\longrightarrow$ ^{113}Cd (stable)

(v) short $\xrightarrow{\beta^-}$ ^{93}Sr (8 m) $\xrightarrow{\beta^-}$ ^{93}Y (10.1 h) $\xrightarrow{\beta^-}$ ^{93}Zn (9.5×10^5 y)

(vi) ^{90}Sr (28 y) $\xrightarrow{\beta^-}$ ^{90}Y (64 h) $\xrightarrow{\beta^-}$ ^{90}Zr (stable)

(vii) short $\xrightarrow{\beta^-}$ ^{83}Se (25 m) $\xrightarrow{\beta^-}$ ^{83}Br (2.4 h) $\xrightarrow{\beta^-}$ ^{83}Kr (stable)

(viii) ^{82}Br (35.34 h) $\xrightarrow{\beta^-}$ ^{82}Kr (stable)

(ix) short $\xrightarrow{\beta^-}$ ^{73}Ga (4.8 h) $\xrightarrow{\beta^-}$ ^{73}Ge (stable)

(x) short $\xrightarrow{\beta^-}$ ^{72}Zn (46.5 h) $\xrightarrow{\beta^-}$ ^{72}Ga (14.1 h) $\xrightarrow{\beta^-}$ ^{72}Ge (stable)

In general, the decay of the nuclides having high activities was followed in the end-window proportional counter, whereas the low activities of several nuclides were measured in the low-level background beta counter. The multi-component activities were measured over three to four half-lives of the long-lived component with about 8 to 10 readings of the count rates for every period of each half-life.

Activities of different nuclides at the end of bombardment were obtained by resolving into different half-life components by the use of the CLSQ decay curve analysis programme (67).

The cesium activities were usually measured in the

end-window counter, and the activity of ^{136}Cs was obtained easily. The activities of ^{134}Cs (2.05 yr) and ^{137}Cs (30 yr) were quite small compared to that of ^{136}Cs. Therefore, the cesium activities were also measured in the low-background counter and an attempt was made to obtain the activities of ^{134}Cs and ^{137}Cs by the CLSQ decay curve analysis programme. Because of the low activity of these nuclides, especially in the catcher foils, no meaningful results could be obtained for these nuclides. However, an average of the results of ^{136}Cs measured by end-window and low-background counters was taken.

The activity of ^{111}Ag was measured after the complete decay of 3.2-hour ^{112}Ag and 5.3-hour ^{113}Ag. The energetic beta radiations from ^{112}Ag, 54% of which decay by emitting 3.94 MeV beta rays and 22% by 3.35 MeV beta rays, were separated from 2 MeV beta rays emitted from ^{113}Ag (5.3 hr), using an aluminum absorber of thickness 1100 mg/cm^2. It should be mentioned that the beta radiations (1.05 MeV and 0.69 MeV) of ^{111}Ag are completely stopped by this absorber. As the absorber reduces the count rate considerably, the low-background beta counter was used in this case. The activities of silver samples were also counted in end-window counter without using any absorber, for gross beta activities from ^{113}Ag, ^{112}Ag, and ^{111}Ag. The count rates of the samples were followed for about 30 days and the activities were resolved into three components of 3.2 hour, 5.2 hour and 7.5 days half-lives.

The activities of ^{113}Ag were thus obtained.

The activities of yttrium and gallium samples were measured by both end-window and low background beta counters and resolved into respective half-life components by the CLSQ programme. The activities of ^{93}Y and ^{73}Ga were taken from both counter measurements and the results were averaged. Because of the low activities of 64-hour ^{90}Y and 14.1-hour ^{72}Ga, the activities of these nuclides from end-window counter measurements could not be resolved accurately, and therefore, the results of these nuclides were obtained from the low background beta counter measurements. Moreover, the formation cross sections of these nuclides are very low at lower bombarding energy and therefore, could not be detected with accuracy.

The 2.4-hour ^{83}Br nuclide was detected in the end-window proportional counter and the 35.34-hour ^{82}Br nuclide in the low-beta counter.

III. RESULTS

III-1 Treatment of Data

(a) The count rates of each of the nuclides at the end of bombardment, as given by the CLSQ programme, were corrected for the chemical yields, and also aliquot factor in the case of the target sample. There was no need for self-absorption corrections as the weights of the samples of the target and the catcher foils did not vary significantly. Since we are interested in the relative activities of the different foils, self-absorption was taken to be the same in all samples.

(b) In the 'integral range' experiments, the fractions of the recoiling atoms in the forward, backward and perpendicular directions are important. From the activities of the forward (A_F), the backward (A_B) and the target (A_T) foils, the fractions of the recoiling atoms in the forward (F), the backward (B) directions (forward-backward experiments), and in the perpendicular (P) directions (perpendicular experiments), were calculated as follows:

$$F = \frac{A_F}{(A_F + A_B + A_T)} \qquad \text{(III-1)}$$

$$B = \frac{A_B}{(A_F + A_T + A_B)} \qquad \text{(III-2)}$$

$$P = \frac{A_U + A_D}{2(A_U + A_D + A_T)} \qquad \text{(III-3)}$$

where A_U and A_D are the activities in the "up" and "down"

catcher foils. The F, B, and P quantities are then multiplied by thickness of the target, W in milligrams per square centimeter, to obtain the more relevant quantities FW, BW, and PW.

(c) The formation cross sections of the fission products were assumed to be constant throughout the target. This is not true for products having steep excitation functions, and corrections for this effect have been considered by Porile (68) and more recently by Ewart et al. (69). No correction was made for this effect in this work, because this was much smaller than the uncertainty in the excitation functions and the beam spread.

(d) The quantities FW, BW, and PW have to be corrected for scattering and edge effects. Scattering effects arise from the differences in scattering of recoil products at the interface of the aluminum catcher and the uranium target. Since the ranges of the recoil products in uranium are measured, ideally the catcher foil should have been uranium; but this is not practically feasible. Panontin and Sugarman (26) have obtained an empirical relationship to correct for this scattering effect from range measurements of fission products using aluminum and lead catcher foils. Based on the data of Niday (31) and those of Panontin and Sugarman (26), they gave the following relationship:

$$(F,\ B \text{ or } P)_{Pb} = [0.922 + 3.4 \times 10^{-4} A] \times [F,\ B \text{ or } P]_{Al} \qquad \text{(III-4)}$$

where the subscripts Pb and Al refer to the quantities measured with Pb and Al catchers respectively. A is the mass number of the recoiling atom. In Eqn. III-4, it is assumed that the scattering effect is the same in both lead and uranium.

The edge effect arises from the fragments recoiling from the surface of the target edges, which increases the total activity in the catcher foils and hence the apparent range in the target material. Recoils originating from the target edge are neglected in deriving the equations III-5 to III-7 shown later for analyzing recoil data from thick-target experiments.

Assuming that the number of recoils escaping from a surface is proportional to its area and the beam intensity of the particles bombarding the surface, Panontin and Sugarman (26) have obtained a value of 0.97 for the correction factor for the edge effect, resulting from the use of a 0.003" thick uranium foil instead of a .001" thick uranium foil.

Since we used .003" thick uranium foil, the overall correction due to scattering and edge effects was obtained by multiplying the FW, BW, and PW values by the product of 0.97 and the value given by Eqn. III-4. The corrected FW, BW, and PW values in milligrams/cm^2 uranium are presented in suitable combinations, in Table III.

TABLE III

Recoil Properties of Measured Nuclides[a]

Nuclide[b]	E_p (MeV)	$2W(F+B)^c$ (mg/cm^2)	4WP (mg/cm^2)	W(F-B) (mg/cm^2)
^{136}Cs(I)	85	8.50±.08(2)	8.25±.05(3)	.291±.038
	70	8.61	8.29±.06(2)	.260
	55	8.62±.08(2)	8.23	.200±.038
	40	8.68±.12(2)	8.24±.09(3)	.203±.060
	25	8.65±.07(2)	8.22±.11(2)	.180±.040
^{113}Ag(C)	85	9.67±.28(2)	9.88±.36(2)	.384±.140
	70	9.35±.22(2)	9.30	.280±.110
^{112}Ag(I)	85	9.61±.10(2)	9.34±.12(2)	.373±.048
	70	9.52±.09(2)	9.33±.08(2)	.289±.014
	55	9.62±.06(2)	9.25±.05(2)	.270±.023
	40	9.70±.12(2)	9.38±.24(2)	.190±.048
^{111}Ag(C)	85	9.95±.08(3)	9.79±.16(2)	.310±.040
	70	9.92±.10(2)	9.75±.09(2)	.250±.050
	55	9.96±.10(2)	9.74±.08(2)	.240±.045
	40	9.89±.11(2)	9.70	.193±.060
	25	9.91±.14(2)	9.65	.213±.070
^{93}Y(C)	85	11.29±.06(3)	11.08±.18(3)	.309±.030
	70	11.25±.09(2)	11.12±.09(2)	.299±.040
	55	11.36±.08(2)	11.02±.20(2)	.249±.042
	40	11.39±.08(2)	11.06	.200±.034
	25	11.37±.10(3)	10.95±.13(2)	.190±.038
^{90}Y(I)	85	10.23	9.90	.342
^{83}Br(C)	85	11.70	11.40	.320
^{82}Br(I)	85	11.51	11.22	.370
^{73}Ga(C)	85	12.45±.12(3)	12.05	.360±.060
	70	12.48±.10(2)	12.09±.12(2)	.299±.048
	55	12.57±.18(2)	11.95±.15(2)	.301±.086
	40	12.46±.11(2)	11.98	.265±.049
	25	12.55	12.12±.18	.180
^{72}Ga(I)	85	12.13±.13	11.78	.410±.070

(a) Corrected for scattering and edge effects.

(b) C and I indicate the nuclides measured either cumulatively (C) or independently (I).

(c) The number in parentheses at the end of columns 3 and 4 indicate the number of experiments performed. The results performed only once are reported without any number.

III-2 Analysis of Data

The analysis of the experimental data obtained from thick target experiments is usually made on the basis of equations given by Winsberg (70) and Sugarman et al. (21). Sugarman's equations were used for the analysis of our results. These equations are derived on the basis of a vector model described briefly in Section I and with the following assumptions:

(i) the fission of a fissioning nucleus with an impact velocity v in the moving frame yields fission products with the average velocity V, (ii) the components of v are $v_{||}$ and $v_{\perp}$ corresponding to the parallel and perpendicular directions to the proton beam, (iii) the angular distribution of the fission products in the moving frame is symmetric about 90° to the beam and of the form $a + b\cos^2\theta$ where θ is the polar angle between the direction of the moving fragment and the incident beam, (iv) the mean range R of a fragment moving with velocity V is given by $R = kV^N$ where k and N are empirical constants, and (v) the value of $\eta = v/V$ is far less than unity. With these assumptions, Sugarman et al. (21) gave the following equations relating the measured FW, BW, and PW values of R, η and b/a.

$$2W(F+B) = \left\{\frac{R}{1+\frac{1}{3}b/a}\right\}\left\{1+\left(\frac{b/a}{2}\right)+\eta_{||}^{\,2}\left[\frac{(N+1)^2}{4}+(b/a)\left(\frac{N-1}{2}\right)\left(\frac{2N+3}{6}\right)\right]\right.$$

$$\left.+\eta_{\perp}^{\,2}\left[\frac{(N^2-1)}{8}+(b/a)\left(\frac{N-1}{2}\right)\left(\frac{N+3}{12}\right)\right]\right\} \qquad \text{(III-5)}$$

$$W(F-B) = \left\{\frac{R}{1+\frac{1}{3}b/a}\right\}\left\{\eta_{||}\left[\left(\frac{N+2}{3}\right)+ (b/a)\left(\frac{3N+2}{15}\right)\right]\right\} \quad \text{(III-6)}$$

$$4WP = \left\{\frac{R}{1+\frac{1}{3}b/a}\right\}\left\{1 +\left(\frac{b/a}{4}\right) + \eta_{||}{}^2\left[\frac{(N-1)}{8}\right]\left[(N+1)+(b/a)\left(\frac{N-1}{2}\right)\right]\right.$$

$$\left. + \eta_{\perp}{}^2\left[\frac{(N+1)}{16}\right]\left[(3N+1)+(b/a)\left(\frac{N+3}{2}\right)\right]\right\} \quad \text{(III-7)}$$

The above equations are correct to first order in b/a and second order in η. Eqn. III-7 ignores the 10° tilt of the foils relative to the proton beam. The momentum transfer to the fissioning nucleus and the fission products due to the evaporation of particles has been ignored.

In order to evaluate R, $\eta_{||}$, and b/a, an iterative procedure was used as suggested by Sugarman et al. (21). The procedure consisted of calculating an approximate value of R from Eqn. III-5, ignoring $\eta_{||}$, $\eta_{\perp}$, and b/a. An approximate value of $\eta_{||}$ is calculated from Eqn. III-7 ignoring b/a and $\eta_{\perp}$. An average value of b/a is calculated from Eqns. III-5 and III-6, ignoring $\eta_{\perp}$. With all these first approximate values, iteration was repeated to obtain a second set of R, $\eta_{||}$, and b/a values ignoring $\eta_{\perp}$. Iterations were continued until the values of R, $\eta_{||}$, and b/a did not change. Then a value of $\eta_{\perp}$ was obtained from the $\eta_{\perp}$ versus $\eta_{||}$ relationship deduced from Monte Carlo calculations (see Section IV-3). This value of $\eta_{\perp}$ was then introduced into the above equations

and R, $\eta_{||}$, and b/a were again calculated. While the value of b/a did change by a few percent (2 to 3%), the values of R and $\eta_{||}$ remained almost constant. The values of the recoil parameters thus obtained are presented in Table IV for different nuclides at different energies.

III-3 Errors

In all radiochemical studies the errors can be classified into two groups:

(i) Systematic errors and

(ii) Random errors.

The systematic errors are associated with the radioactive decay properties of the nuclides reported in the literature and the counting efficiencies of the counter. These systematic errors are avoided in recoil studies since only the ratios of activities are needed in the final treatment of data.

The random errors are encountered in the determination of disintegration rates (resolution of decay curves, counter back-ground etc.), chemical yields, non-uniformity of target and catcher foils, dilution factors, radioactive purity, self-absorption, and back-scattering of beta radiation in the samples.

The following steps were taken to minimize the random errors encountered in the present work. Where possible, the total number of counts accumulated were about 10^5 and not less than 10^4 in almost all cases. As already mentioned 8 to 10

TABLE IV

Recoil Parameters of Measured Nuclides

Nuclide	E_p (MeV)	R (mg/cm^2)	$\eta_{\parallel}$	$\eta_{\perp}$	b/a
^{136}Cs(I)	85	8.33±.06	.031±.004	.025±.002	.123±.015
	70	8.39±.04	.028±.001	.027±.001	.158±.033
	55	8.36±.03	.022±.003	.019±.002	.197±.045
	40	8.38±.09	.022±.006	-	.223±.022
	25	8.36±.10	.019±.005	-	.219±.036
^{113}Ag(C)	85	9.64±.17	.036±.001	.025±.02	.195±.123
	70	9.31±.08	.027±.007	.024±.02	.095±.020
^{112}Ag(I)	85	9.42±.11	.036±.004	.028±.010	.133±.026
	70	9.33±.16	.028±.002	.016±.008	.085±.046
	55	9.36±.06	.028±.003	.012±.002	.151±.013
	40	9.49±.19	.018±.004		.140±.062
^{111}Ag(C)	85	9.84±.17	.028±.004	.018±.002	.063±.040
	70	9.80±.09	.029±.006	.017±.002	.066±.003
	55	9.81±.09	.022±.004	.012±.002	.090±.024
	40	9.76±.03	.018±.006	-	.078±.056
	25	9.78±.05	.019±.007	-	.109±.064
^{93}Y(C)	85	11.15±.10	.025±.003	.015±.001	.075±.02
	70	11.16±.09	.020±.003	.012±.002	.057±.014
	55	11.13±.16	.020±.003	.011±.002	.125±.055
	40	11.17±.03	.016±.003	-	.122±.032
	25	11.09±.06	.015±.003	-	.158±.010
^{90}Y(I)	85	10.01	.031	.013	.133
^{83}Br(C)	85	11.50	.025	.013	.105
^{82}Br(I)	85	11.31	.029	.011	.098
^{73}Ga(C)	85	12.18±.04	.026±.005	.011±.002	.136±.044
	70	12.22±.11	.022±.004	.011±.002	.131±.015
	55	12.15±.13	.022±.006	-	.208±.024
	40	12.08±.08	.017±.003	-	.165±.032
	25	12.26±.12	.013±.002	-	.146±.070
^{72}Ga(I)	85	11.89±.04	.030±.005	-	.117±.047

readings of the count rates for every period of each half-life of a nuclide, were taken to minimize the error in the CLSQ decay curve analysis (67). As mentioned earlier in chemical procedures, proper care was taken in preparing the samples in order to minimize the self-absorption and dead-time corrections. In several cases a given sample was alternated between 2 to 3 counters to get independent count rates from different instruments.

The spread in the bombarding energy as reported by the Foster Radiation Laboratory Group of McGill University was $\pm$ 2 MeV.

Duplicate and triplicate experiments were performed for most cases. The errors quoted in columns 3, 4 and 5 of Table III are the standard deviation (triplicate determinations) or the mean deviation (duplicate determinations). Nuclides measured only once are listed without error. The number of determinations made of each nuclide is given in parentheses. Errors for the range, R, velocity parameter, η, and anisotropy parameter b/a as quoted in Table IV have been calculated on the basis of the standard deviation or mean deviation given in Table III.

IV. DISCUSSION

IV-1 General

From the present recoil experiments we have obtained three important quantities, given in Table IV, namely the range R, the velocity parameter η, and the anisotropy parameter b/a for the angular distribution of the recoil products. First, kinetic energies of the measured fission products will be derived from the range R using a suitable range-energy relationship. These will be compared with other published data and discussed. From kinetic energies, the fission velocity of the recoil will be obtained which will then be used to give the components of initial impact velocity, $v_{||}$ and $v_{\perp}$ ($\eta_{||} = v_{||}/V$ and $\eta_{\perp} = v_{\perp}/V$). The cascade calculations of Chen et al. (12) will be used to calculate the deposition energy of the fissioning nucleus. Finally some observations will be made about the observed anisotropy of the angular distribution of different recoil products.

IV-2 Average Range and Kinetic Energies of Fission Products

The average ranges, R, as tabulated in Table IV, are of expected magnitudes as compared to the values reported by other authors (21,27,31,35-37,47,48). It is observed that the ranges do not change with the bombarding energy. The ranges of ^{111}Ag agree with that reported by Alexander et al. (27) for 23-MeV deuteron fission of ^{238}U. The range of ^{111}Ag for 23-MeV deuteron fission is 9.74 mg/cm^2 in uranium (27). The ranges of Ga, Br

and Ag isotopes measured in the present work agree well with those of Noshkin and Sugihara (35) who reported the ranges in mg/cm^2 of uranium for ^{72}Ga = 11.99, ^{73}Ga = 12.42, ^{83}Br = 11.90, ^{82}Br = 11.34 and ^{111}Ag = 9.50 (corrected for scattering and edge effects) formed in the fission of ^{238}U by 150-MeV protons. The ranges of fission products in the present work are in general about 3-4% higher than those of Niday (31) in thermal neutron fission of ^{235}U. All these lead to the conclusion that the ranges of fission products are independent of bombarding energy.

It is noted, in Table IV, that the range of ^{72}Ga (semi-shielded) is slightly smaller than that of ^{73}Ga (cumulative). Similarly the ranges of ^{112}Ag (semi-shielded) are less than that of ^{111}Ag (cumulative). Niday (31) first observed that the ranges of shielded nuclides ^{86}Rb and ^{136}Cs were shorter than the average ranges of the neighbouring mass chains and this was further confirmed by Brown and Oliver (30) for ^{136}Cs. Nakahara (71) explained the short range of the shielded nuclide ^{136}Cs, in terms of its formation from a fission process involving lower kinetic energies.

As already mentioned in Section I-4, the kinetic energy of a fission product can be obtained from the measured ranges by the use of a suitable range-energy relationship. The merits and demerits of several range-energy relationships as proposed by various authors have been discussed in Section I-4. In the present work, we have used the range-energy relationship of Lindhard et al. (34), suitably simplified by

Noshkin and Sugihara (35).

The equation by Lindhard et al. provides a general framework for the conversion of an experimental range to the kinetic energy. The modified form, by Noshkin and Sugihara, is useful because of its simplicity. Although both electronic and nuclear stopping are considered in the general formulation of the cumbersome equation of Lindhard et al. for the stopping of heavy ions, that part of the equation responsible for nuclear stopping accounts for only about 10% of the total stopping in the case of fission, even after the kinetic energy is reduced by about 70% (72). The term responsible for nuclear stopping (see equation I-8) is ignored in deriving the simplified version of the equation of Lindhard et al. The range-energy equation as given by Noshkin and Sugihara and used in the present work is given as

$$\rho(\varepsilon) = \left(\frac{1.3}{k}\right)\varepsilon^{1/2} \qquad \text{(IV-1)}$$

where $\rho(\varepsilon)$ and ε are dimensionless measures of range and energy and k is a constant. The relationships between ρ and R, ε, and the kinetic energy have been explained in detail in Section I-4. After substitution of known quantities into the above-mentioned equation, the following range-energy relationship for fission fragments moving in uranium is obtained

$$T = \frac{466.41 \times Z^{7/3} R^2}{A(Z^{2/3} + 20.4)^3} \qquad \text{(IV-2)}$$

where T is kinetic energy in MeV, Z and A refer to the charge and mass respectively of the recoiling fission product and R is in mg/cm^2. In the conversion of the range to the kinetic energy by using equation (IV-2), it was assumed that the values of $\bar{v}^2$ and $\overline{v^2}$ are equal. In fact, this assumption is valid for neutron-excessive fission products formed in thermal neutron fission (30) and in GeV-proton fission (54). However, a correction of about 10% is necessary for neutron-deficient fission products formed from high-energy fission (54). In the present work, since the observed recoil products are neutron-excessive, the assumption that the dispersion of $\bar{v}$ is small compared to $\bar{v}^2$, is probably valid.

The charge dependence of the above range-energy relationship is apparent. For a shielded or semi-shielded nuclide the charge of a fission product is the same as that of the measured independent nuclide. However, for a cumulatively-formed nuclide, the average charge <Z> is given as

$$\langle Z \rangle = \frac{\Sigma f_i Z_i}{\Sigma f_i} \qquad \text{(IV-3)}$$

where f_i is the fractional yield of the i^{th} member of the isobaric chain, and isobaric nuclides of charges less than and equal to that of the observed nuclide, are considered in the summation.

The fractional yield f_i is obtained from the charge dispersion curves of fission products and it is assumed to have a Gaussian distribution (73,74) of the form

$$P(Z) = \frac{1}{\sqrt{c\pi}} \exp\left[\frac{-(Z-Z_p)^2}{c}\right] \qquad \text{(IV-4)}$$

where Z_p is the most probable charge of the isobaric chain. The standard deviation c is related to the full-width at half-maximum d_i by the relation $c = 0.361 d_i^2$ (75). Substituting in equation (IV-3) the fractional chain yield of Z_i the nuclear charge of the nuclide of interest, is thus obtained as

$$f_i(Z_i) = \frac{(0.940)}{d_i} \exp\left[\frac{-.277(Z_i-Z_p)^2}{d_i^2}\right] \qquad \text{(IV-5)}$$

The values of the full-width at half-maximum, d_i, of the charge dispersion curves for masses 130-144 in ^{238}U fission by protons of energy 20-85 MeV have been given by Davies and Yaffe (76) and Parikh et al. (77). The values of d_i in the mass region of 90-96 in the proton fission of ^{238}U at 25-85 MeV have been reported by Khan (78). For ^{93}Y we have used Khan's data. For silver isotopes near symmetric fission and gallium and bromine isotopes in the light mass region no charge dispersion studies have been reported in this energy range. In the absence of any data for d_i, the values of Davies and Yaffe have been chosen arbitrarily for the above-mentioned nuclides. However, it can be shown that although $f_i(Z_i)$ changes with the variation in d_i, the average charge $\overline{Z}$ remains almost constant. The values of d_i from Davies and Yaffe (76) and Khan (78) are shown in Fig. 3.

The most probable charge Z_p for ^{93}Y could be obtained

FIGURE 3

Full-Width at Half-Maximum (FWHM) versus proton bombardment energy (E_p).

—o— Data from Davies and Yaffe (76).

—o— Data from Khan (78).

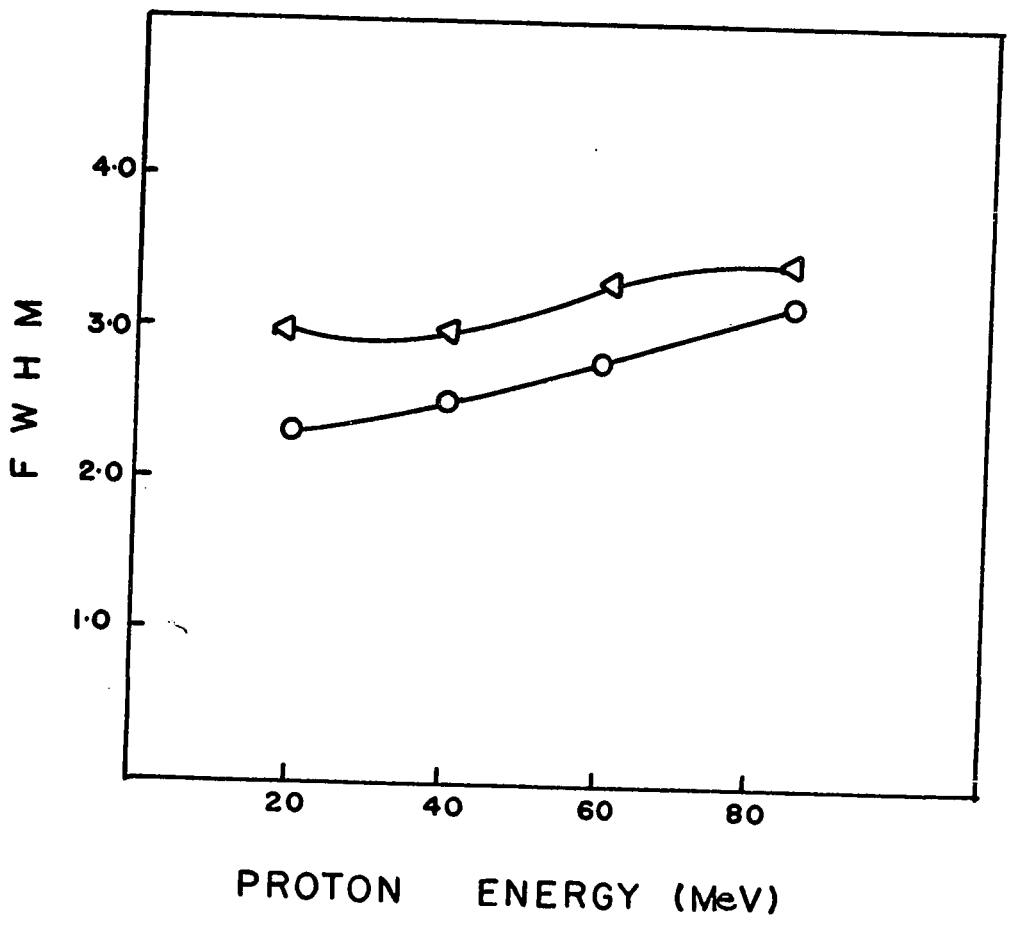
4·0
3·0
2·0
1·0
F W H M
20
40
60
80
PROTON ENERGY (MeV)

from Khan (78). But to be consistent in our analysis, we have used Z_p calculated on the basis of the Equal Charge Displacement (ECD) and the Unchanged Charge Division (UCD) postulates (79). These are given as

$$Z_p(\text{ECD}) = \frac{1}{2}\left[Z_f + Z_A - Z_{(A_f-A)}\right] \qquad \text{(IV-6)}$$

$$Z_p(\text{UCD}) = \frac{Z_f A}{A_f} \qquad \text{(IV-7)}$$

where Z_f and A_f are the charge and mass numbers of the fissioning nucleus. Z_A is the most stable charge associated with mass A. The values of A_f and Z_f were obtained from Vegas cascade calculations (12) as will be explained later. The values of Z_f were taken to be the same as those of residual nuclei given by the Vegas calculations, as proton evaporation was assumed to be small enough to be neglected. On the other hand, the residual nuclei with proper excitation energy from the cascade calculation were subjected to neutron evaporation and fission competition. The mass of the average fissioning nucleus A_f was obtained by weighting each fissionable mass along the evaporation chain with its fissionability parameter.

With the above information we calculated <Z> for cumulatively-formed fission products using Z_p values obtained from both UCD and ECD methods. The appropriate values of <Z> for cumulative fission products and Z for independent products were inserted into equation IV-2. Using the range values from

Table IV, the kinetic energies of different fission products were calculated and these are tabulated in Table V. The average charge <Z> of the cumulatively-formed fission products obtained by UCD and ECD methods are also included in Table V. The charges of the independently-formed fission products are given in column 4 and their kinetic energies are listed in column 6. Column 7 lists the values of cascade deposition energies for the observed fission products. In Section IV-3, the calculation of cascade deposition energy, E*, is explained in detail.

The average kinetic energies as calculated by equation (IV-2) using the average <Z> obtained by both ECD and UCD hypotheses have errors not exceeding 5%.

From Table V one sees that for ^{113}Ag and ^{111}Ag the average charge <Z> from the UCD method is higher than that from the ECD method by about 1 charge unit at higher energies, whereas at lower energies both postulates predict the same value of <Z>. For ^{93}Y the average charge <Z> from UCD is slightly higher than that from ECD at higher energies, and the difference between the two calculations disappears at lower energies. On the other hand, the converse trend is observed in the case of ^{73}Ga. Despite these discrepancies in the values of <Z>, the kinetic energies obtained by both UCD and ECD methods agree very well with each other within the experimental error. We have, however, arbitrarily chosen the values of the UCD method for future discussion.

TABLE V

Kinetic Energy and Cascade Deposition Energy

Nuclide	E_p (MeV)	ECD ⟨Z⟩	UCD ⟨Z⟩	ECD T (MeV)	UCD T (MeV)	E* (MeV)
^{136}Cs (I)	85		55		64.6±1.0	42.2 ± 9.0
	70		55		65.6± .6	40.6 ± 1.2
	55		55		65.1± .4	33.7 ± 8.6
	40		55		65.5±1.4	38.2 ± 8.0
	25		55		65.1±1.5	31.6
^{113}Ag (C)	80	45.1	46.0	76.3±3.0	78.9±3.0	58.7 ± 7.2
	70	45.1	45.8	71.6±4.0	73.4±4.0	39.4 ± 6.8
^{112}Ag (I)	85		47		79.0±1.8	69.4 ± 8.8
	70		47		77.5±1.8	50.0 ± 2.9
	55		47		78.1± .7	46.2 ± 6.7
	40		47		80.0±3.4	30.1 ± 13.6
^{111}Ag (C)	85	44.3	45.4	79.3±2.2	82.2±2.2	55.8 ± 8.9
	70	44.3	45.2	78.7±1.5	81.1±1.5	40.1 ± 9.2
	55	44.3	44.9	78.8±1.4	80.3±1.4	37.6 ± 8.5
	40	44.3	44.6	78.0± .6	78.7± .6	32.8 ± 12.6
	25	44.3	44.2	78.3±1.3	78.1±1.4	31.6
^{93}Y (C)	85	37.4	37.9	92.5±1.5	94.4±1.6	59.5 ± 6.2
	70	37.4	37.7	92.7±1.3	93.9±1.3	53.2 ± 8.6
	55	37.4	37.5	92.3±2.7	92.8±3.7	42.7 ± 7.4
	40	37.4	37.3	92.9± .4	92.5± .4	32.4 ± 14.8
	25	37.4	37.0	91.6±1.0	90.1± .8	31.6
^{90}Y (I)	85		39.0		82.5	74.7
^{83}Br (C)	85	33.5	33.8	92.3	93.4	64.2
^{82}Br (I)	85		35.0		97.0	82.2
^{73}Ga (C)	85	29.7	29.7	95.9± .6	96.1± .7	77.3 ± 14.6
	70	29.7	29.6	96.5±1.8	95.9±1.7	58.2 ± 10.0
	55	29.7	29.4	95.5±2.0	94.2±2.0	54.4 ± 13.0
	40	29.7	29.3	95.3± .6	93.0± .5	38.4 ± 8.2
	25	29.7	29.1	97.3±2.0	93.8±2.0	31.6
^{72}Ga (I)	85		31		99.8± .7	83.2 ± 7.0

It is interesting to note in Table V that the kinetic energy of any product, independent or cumulative, is independent of the bombarding energy. In order to illustrate this we have accumulated kinetic energy data obtained at different bombarding energies. In addition to the present data, thick-target range measurements in thermal-neutron fission (31) of ^{235}U, 23-MeV deuteron fission of ^{238}U (27) and 720-MeV proton fission of ^{238}U (48) have been reported as well as ranges (in aluminum) for 18-MeV deuteron and 335-MeV proton fission of ^{238}U (80). The ranges have been converted to kinetic energies by Noshkin and Sugihara (35) who did their work at 150 MeV. All these data are summarized in Table VI. It is apparent that no definite dependence of kinetic energies of the fission products on the bombarding energy is evident. Sugarman et al. (21) have, however, found that the kinetic energies decrease, in general, with increasing proton energy particularly for the light-mass and neutron-deficient fission products. Saha and Yaffe (55) also observed a similar decrease in kinetic energies of ^{67}Ni, ^{67}Cu, and ^{72}Zn in the proton fission of ^{238}U at 20-85 MeV. The observed discrepancy between the kinetic energies of ^{72}Ga and ^{73}Ga at 20-85 MeV and 150 MeV cannot be readily explained.

The constancy of kinetic energies of the products at different bombarding energies probably results from the fact that the coulomb energy does not depend on excitation energy, and the average distance between the two charge centres is the

TABLE VI

Kinetic Energies (MeV) of Some of the Fission Products at Different Bombarding Energies

Nuclide	n_{th}	d_{18}	d_{23}	p_{25-85}	p_{150}	p_{335}	p_{450}	p_{720}
^{136}Cs	64.6	-	-	64.6	59.6	-	-	-
^{111}Ag	77.5	80.4	81.5	81.5	81.2	74.9	-	71.6
^{93}Y	98.0	-	-	99.2	-	-	-	-
^{72}Ga	-	-	-	99.8	126.8	-	92.4	-
^{73}Ga	-	-	-	95.0	115.0	-	94.1	-
	(31)	(80)	(27)	(a)	(35)	(80)	(21)	(48)

(a) From the present work.

same at all excitation energies. This will be discussed later in connection with the total kinetic energy release in fission.

In view of the constancy of the kinetic energies of the fission products at 25-85 MeV, we have obtained the average value for each fission product and plotted them against the mass number of the fission product in Fig. 4. As expected, the kinetic energy decreases with increasing mass number. In Fig. 5, we have plotted the kinetic energies versus the neutron-to-proton ratio divided by the mass number, $\frac{<N>/<Z>}{A}$ of the product. The abscissa $\frac{<N>/<Z>}{A}$ was used in order to reduce the effect of the A dependence of kinetic energy for all masses investigated. This type of plot has been suggested for heavy mass region by Hogan and Sugarman (41). It is apparent that the neutron-excess products have much less kinetic energy than the neutron-deficient products. In particular, ^{136}Cs has relatively small kinetic energy. There is evidence in thermal neutron fission (31) that the fission product ^{136}Cs is formed in events involving large distortion and relatively low kinetic energy release. This may be true for ^{136}Cs at the present energies of 25-85 MeV protons also.

Although the range of ^{72}Ga is smaller than that of ^{73}Ga, the kinetic energy of the former is higher than that of the latter. This inconsistency apparently arises from the uncertainty in the average charge, <Z>, used for ^{73}Ga in the

FIGURE 4

Kinetic energy versus mass number. The kinetic energies T of the fission products of mass numbers A, are taken from Table V and the values of T are on the basis of UCD hypothesis.

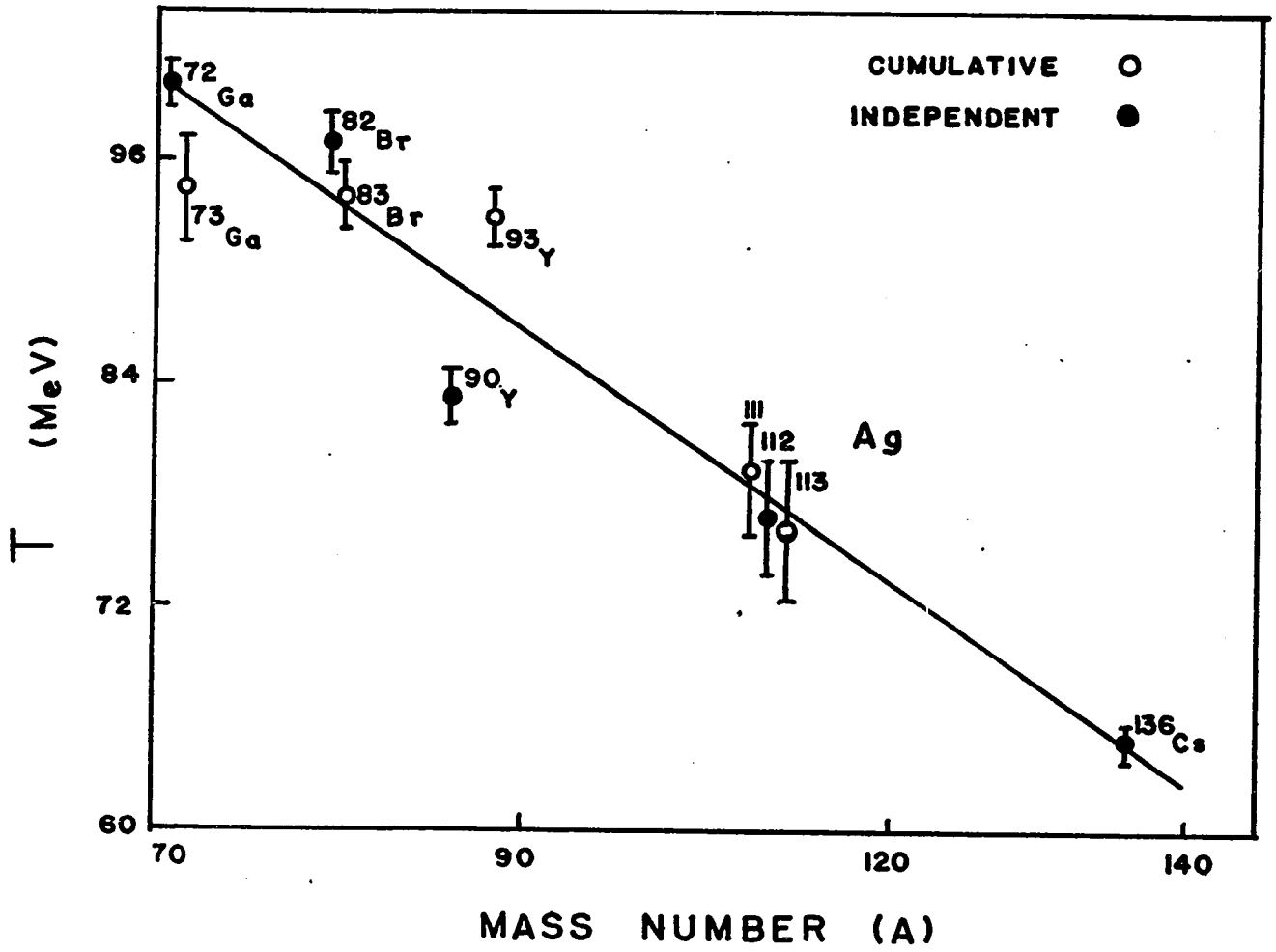
CUMULATIVE
INDEPENDENT
72 Ga
82 Br
73 Ga
83 Br
93 Y
90 Y
111
112
113
Ag
136 Cs
96
84
72
60
T (MeV)
70
90
120
140
MASS NUMBER (A)

FIGURE 5

Kinetic energy versus <N>/<Z>. <Z> and kinetic energy T, are taken from Table V and the values are on the basis of UCD hypothesis.

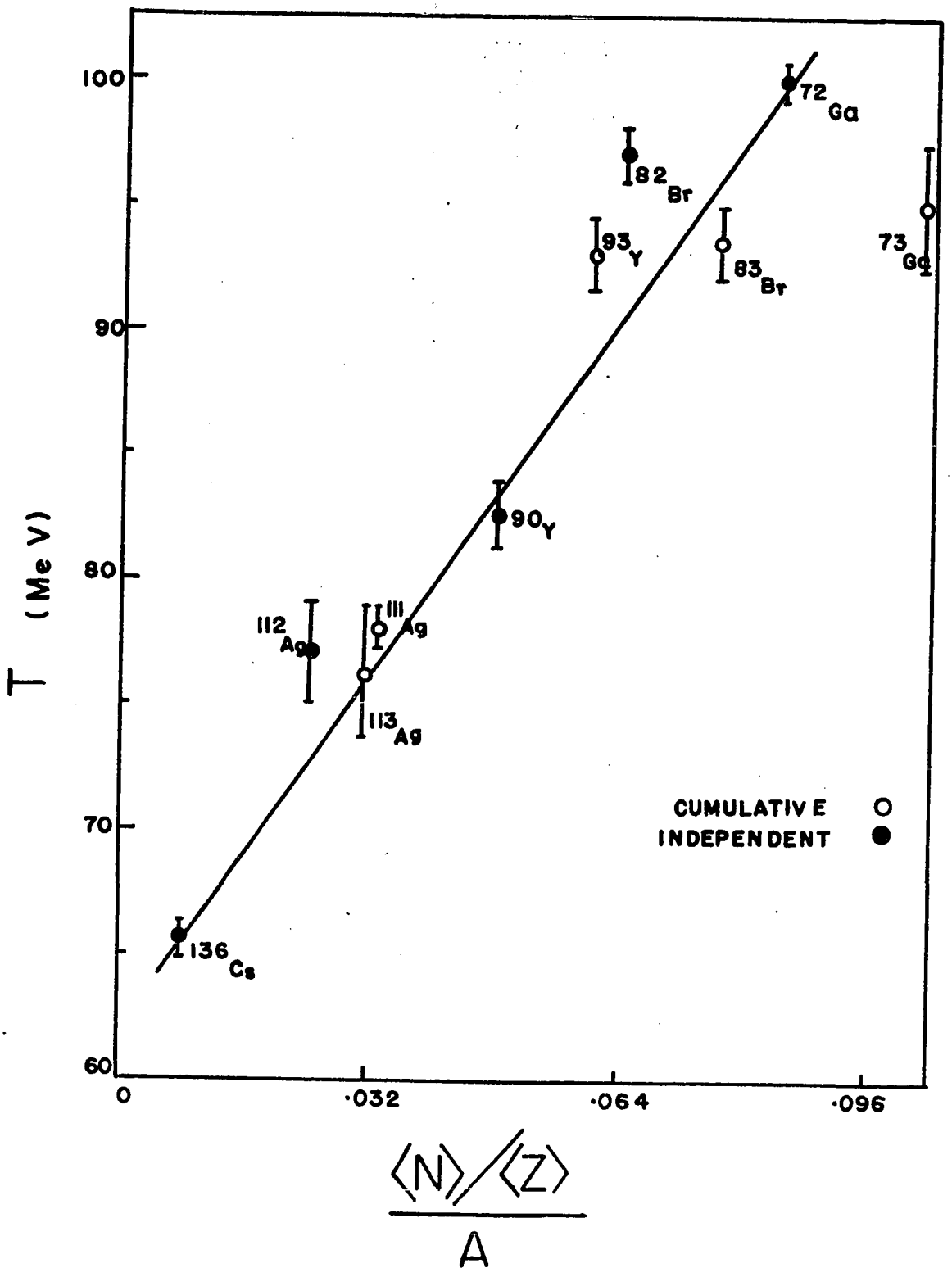
100
90
80
70
60
T (MeV)
0
·032
·064
·096
⟨N⟩/⟨Z⟩ / A
72 Ga
82 Br
93 Y
83 Br
73 Ga
90 Y
112 Ag
111 Ag
113 Ag
136 Cs
CUMULATIVE
INDEPENDENT

calculation of kinetic energy by use of equation (IV-2).

IV-3 Cascade Deposition Energy Leading to a Fission Product

Once the kinetic energy T of a fission product is known, the fission velocity V can be calculated from $T = 0.5 AV^2$. The impact velocity $v_{||}$ can then be calculated by multiplying $\eta_{||}$ given in Table IV by the fission velocity V. From $v_{||}$ one can calculate $p_{||}$, the initial momentum transferred to the target nucleus by the incident proton. In order to obtain the deposition energy E* of the struck nucleus, a relationship between E* and $p_{||}$ is necessary. For this purpose, the cascade calculations[a] of Chen et al. (12) have been used here. This calculation also gives the relation between the momentum transfer along the parallel ($p_{||}$) and the perpendicular ($p_{\perp}$) directions. The details of the calculation have been given in their original paper (12) and only pertinent points will be given below.

In the calculations, the radial density distribution of the nucleus is taken to be a seven-step function with the nuclear radius $r = (1.07 \times A^{1/3} + 2.5)$Fermi and the radius of the central core $c = (1.07 \times A^{1/3} - 2.5)$Fermi. The radius and density of each of the seven regions are chosen in such a way that the whole density distribution ($\zeta(r)$) approximates

[a] I am indebted to Dr. K. Chen for making the computer code available to Dr. G.B. Saha of this laboratory who adapted it to the McGill IBM-360 computer.

the Fermi distribution:

$$\zeta(r) = \frac{\zeta_o}{1 + \exp\left(\frac{r-c}{a}\right)} \qquad \text{(IV-8)}$$

where ζ_o and c are the core density and radius respectively and a is the 'skin thickness' of the nucleus. The momentum distribution of the nucleons in the nucleus is assumed to be that of a degenerate Fermi gas, with the Fermi energy given by:

$$E_{F_i} = (\hbar^2/2m_i)(3\pi^2\zeta_i)^{2/3} \qquad \text{(IV-9)}$$

where the subscript i stands for either protons, or neutrons, m is the nucleon mass, and ζ_i is the density of protons or neutrons. The ratio of proton density to neutron density is assumed to be Z/(Z-A) in all regions.

As a consequence of the variation of Fermi energy, the nuclear potential of the nucleus differs in the various density regions. As a particle crosses one density region into the adjoining region, the kinetic energy changes according to

$$E' = E - (V' - V) \qquad \text{(IV-10)}$$

where the primed and unprimed values correspond to the new and old density regions respectively. The incident particle also changes the radial component of momentum in different density regions. The three elementary differential cross sections for proton-proton, proton-neutron and neutron-neutron interactions are taken from experimental data. The cascade

particles are followed for all struck nucleons until a minimum cut-off energy is reached, taken to be the sum of the neutron and proton binding energies of the struck nucleus. Although the Vegas calculations have the facility of inclusion or exclusion of refraction and reflections of nucleons at the nuclear surface and at assumed boundaries between regions of different potential energy, the reflection and refraction were neglected in the present work. This was based on the fact that at energies of <100 MeV, better agreement with the experimental data was obtained when reflection and refraction were neglected (12). The residual excitation energy is calculated as in Metropolis et al. (8, 9,12) and the recoil momentum is obtained by subtracting the momenta of all outgoing particles from the momentum of the bombarding particle. The residual angular momentum is calculated in an analogous way. The output from the cascade calculations lists the following quantities:

(a) the points of entry of the incident particle in x,y,z coordinates.

(b) Z, A, and E* (excitation energy in MeV) of the residual nucleus.

(c) L, the residual angular momentum in units of $\hbar$ and L_z/L, the fraction of z component of angular momentum.

(d) p_x, p_y, and p_z, the linear momentum components of the residual nucleus and their vector sum p in units of (MeV/c). The directions of the momenta are such that p_z is parallel to

the beam direction ($p_{||}$) and $p_{\perp} = (p_x^2 + p_y^2)^{1/2}$, and (e) serial number of the cascade.

In the present work, calculations were performed for 2000 cascades each for bombardment by protons of energies 40, 55, 70 and 85-MeV on ^{238}U using the IBM-360 computer at the McGill University Computing Centre. The output from the computer was collated for every 8-MeV intervals of residual excitation energy and the corresponding values of E^*/E_{CN} ($E_{CN} = E_{CM} + Q$ where E_{CM} is the centre-of-mass energy and Q is reaction Q of the compound nucleus formation) for the same intervals, were computed. Similarly the average values of $p_{||}/p_{CN}$ (p_{CN} = momentum of the compound nucleus) and $p_{\perp}/p_{||}$ were also calculated for the same 8-MeV intervals of the excitation energy of the residual nuclei. The relationships between $p_{||}/p_{CN}$ and E^*/E_{CN} for 40, 55, 70, and 85-MeV are shown graphically in Figs. 6 and 7. Similarly the relationships between $p_{\perp}/p_{||}$ and $p_{||}/p_{CN}$ are presented in Figs. 8 and 9. The vertical bars in Figs. 6 and 7 represent the standard deviation of the average $p_{||}/p_{CN}$ values about the mean. The horizontal bar represents the width of E^*/E_{CN} corresponding to the 8-MeV interval.

It is seen from Figs. 6 and 7 that the deposition energy increases, although not linearly, with increasing linear momentum transfer. The relationships between E^*/E_{CN} and $p_{||}/p_{CN}$ show almost the same trend at all bombarding energies. Furthermore, Figs. 8 and 9 indicate that the ratio

FIGURE 6

Momentum transfer in the parallel direction versus cascade deposition energy for 85 and 75-MeV proton irradiation of ^{238}U.

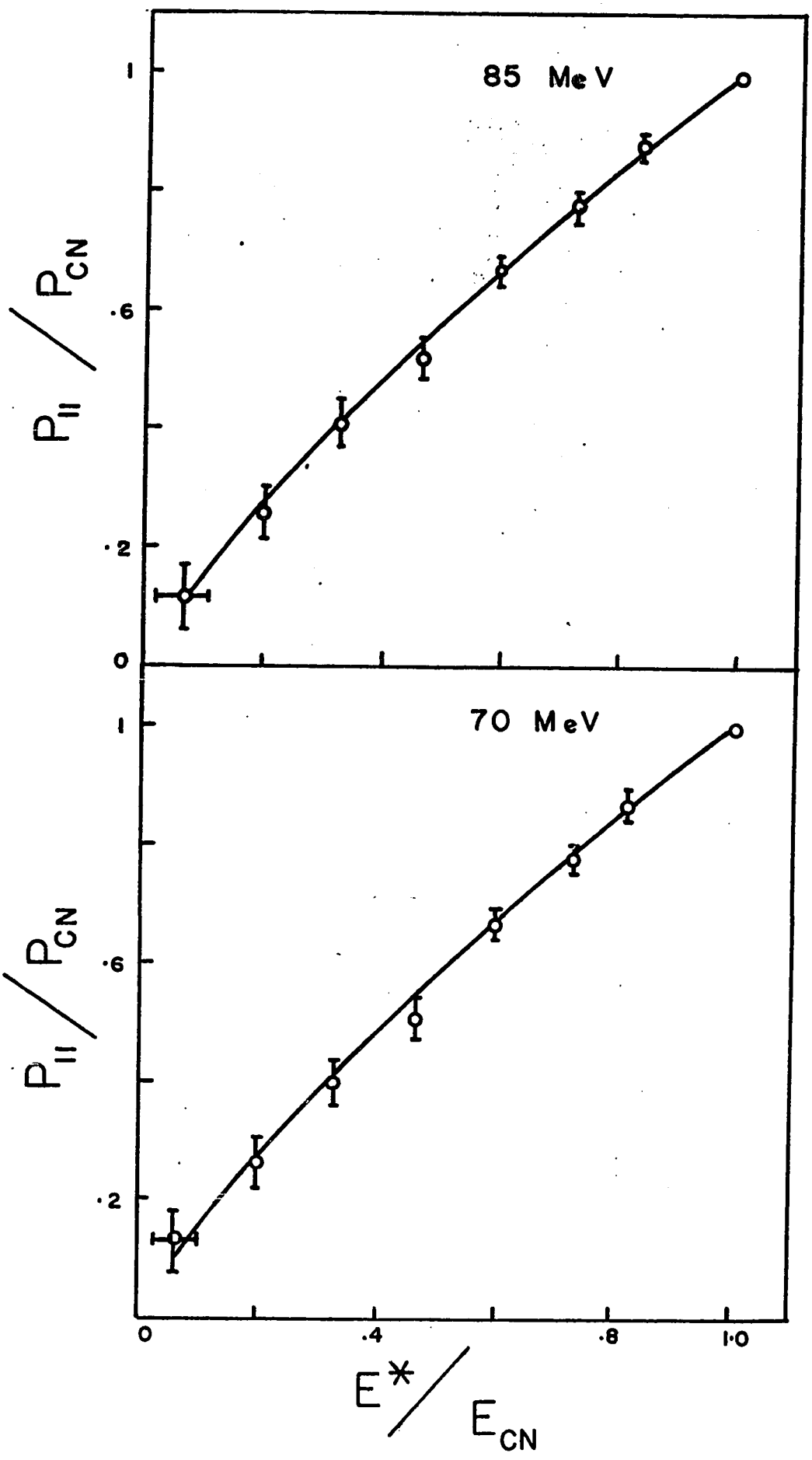
85 MeV
70 MeV
P_{II} / P_{CN}
E^* / E_{CN}
0
.2
.6
1
.4
.8
1.0

FIGURE 7

Momentum transfer in the parallel direction versus cascade deposition energy for 55 and 40-MeV proton irradiation of ^{238}U.

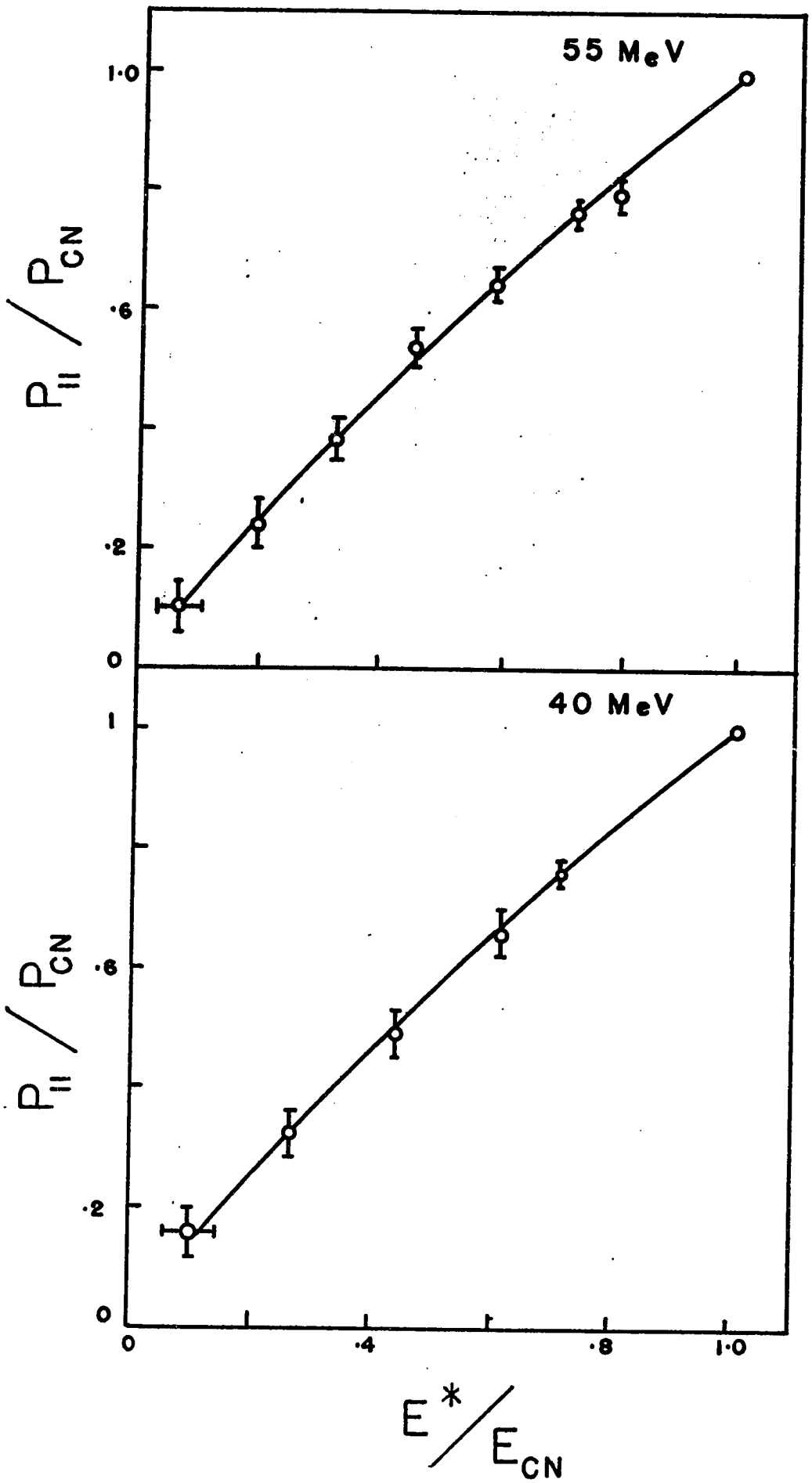
55 MeV
40 MeV
P_{II} / P_{CN}
E^* / E_{CN}
0
·2
·4
·6
·8
1·0
1

FIGURE 8

Momentum transfer in the perpendicular direction versus momentum transfer in the parallel direction for 85 and 70-MeV proton irradiation of ^{238}U.

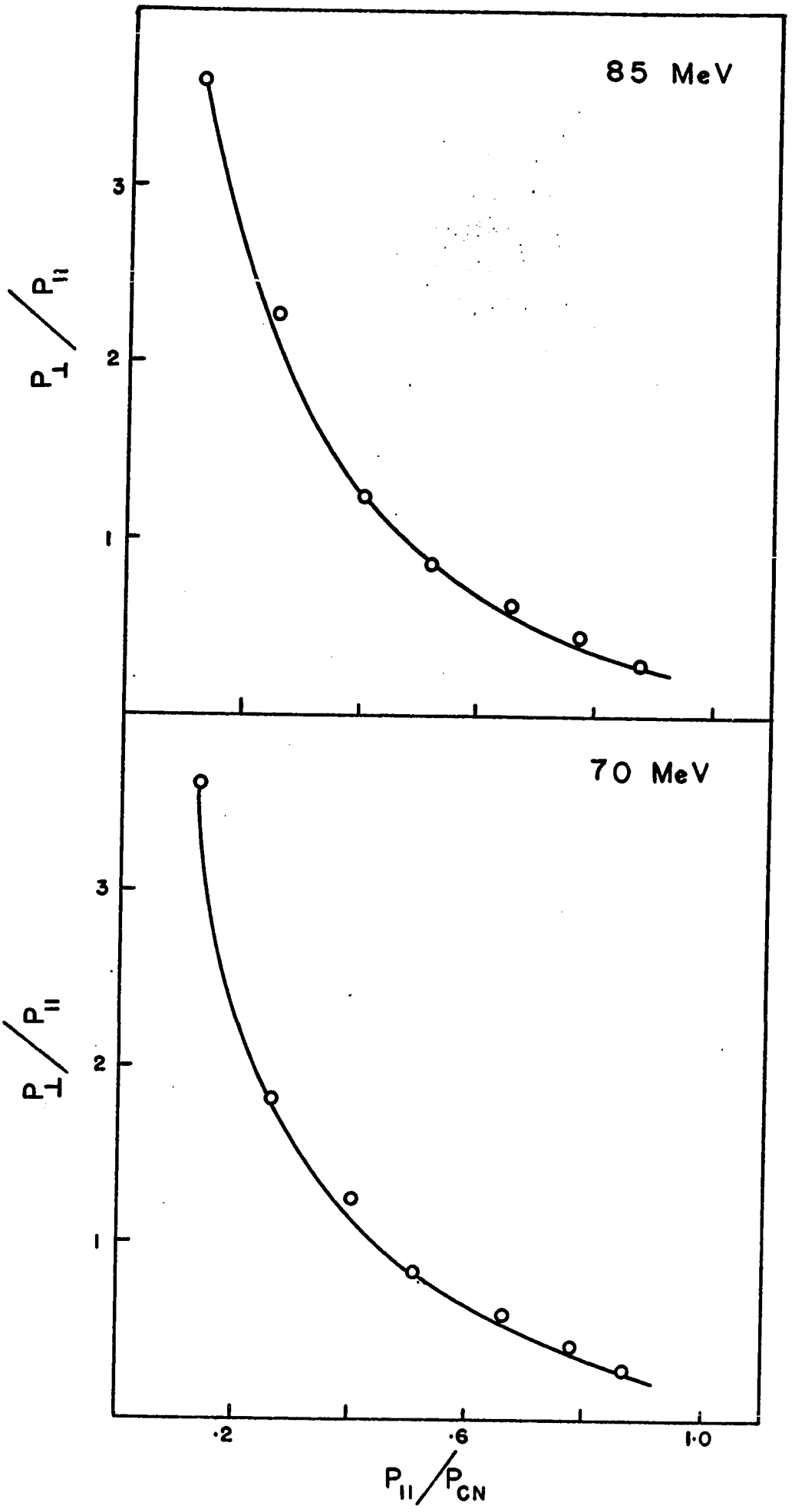
85 MeV
70 MeV
$P_\perp / P_{||}$
3
2
1
·2
·6
1·0
$P_{||} / P_{CN}$

FIGURE 9

Momentum transfer in the perpendicular direction versus momentum transfer in the parallel direction for 55 and 40-MeV proton irradiation of ^{238}U.

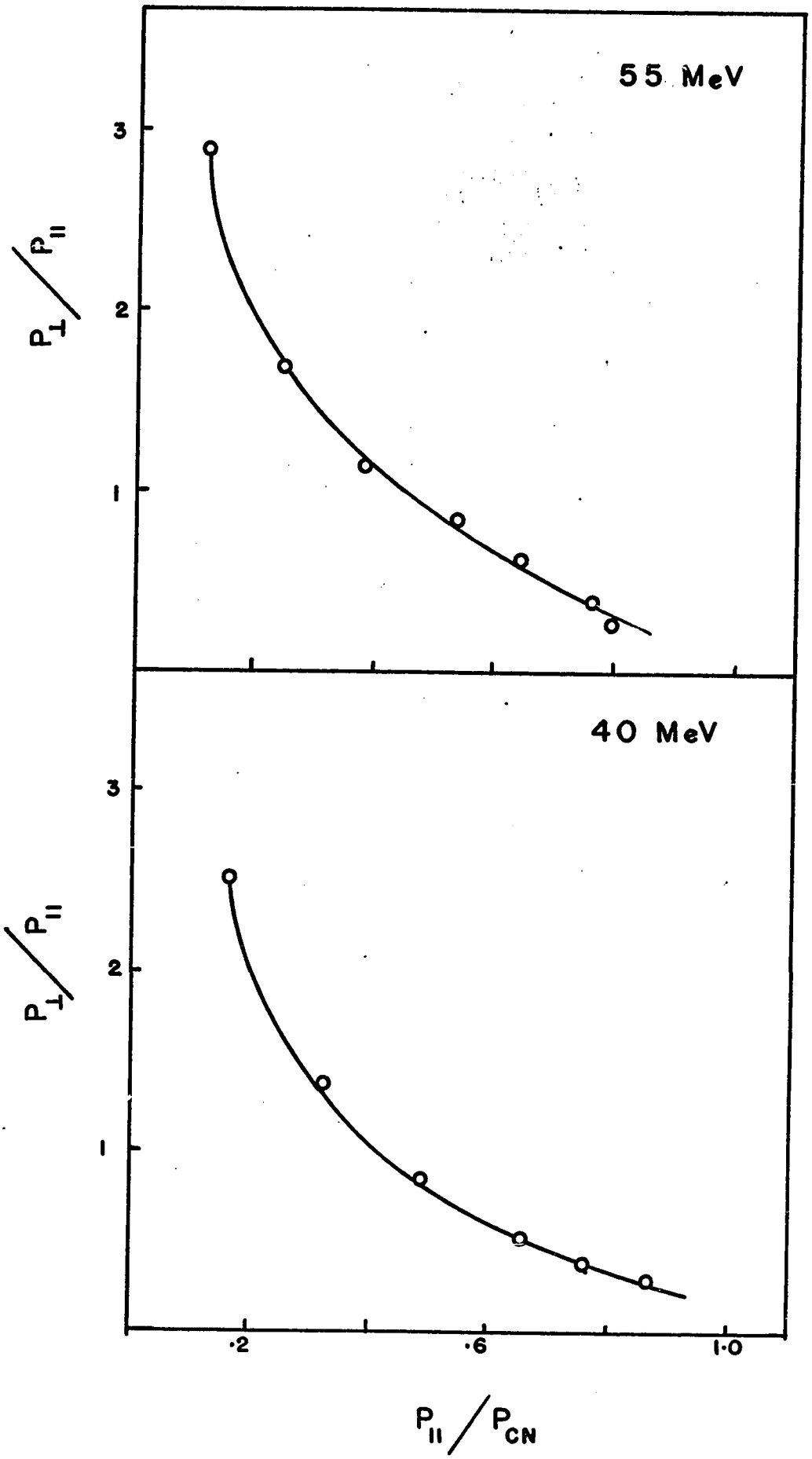
55 MeV
40 MeV
$P_\perp / P_{II}$
3
2
1
·2
·6
1·0
P_{II} / P_{CN}

of the perpendicular and parallel momenta, decreases rapidly with increasing values of the parallel momentum transfer.

The experimental values of p_{11} as obtained in the earlier part of this section were used to determine E* from Figs. 6 and 7, and similarly $p_{\perp}$ was obtained from Fig. 8 and 9 for each fission product. The values of E* are included in Table V. The values of $\eta_{\perp}$ are calculated from $p_{\perp}$ for each nuclide and tabulated in Table IV. The cascade calculation for 25 MeV bombardment indicates mostly compound nucleus formation and therefore, the excitation energy of the compound nucleus has been quoted as 31.2 MeV in Table V.

The values of E* have been plotted versus Z_A - <Z> in Figs. 10 and 11 for each fission product where Z_A is the most stable charge for the mass of interest. Since the complementary fragments do not necessarily have the <N>/<Z> (except where the UCD mechanism is valid), Z_A - <Z> will be a more relevent parameter than <N>/<Z> in obtaining information about the deposition energy dependence in the formation of different products. For reasons given earlier, no data for 25 MeV bombardment have been shown graphically.

It is seen from Figs. 10 and 11 that despite the scatter of experimental points, the average deposition energy is almost constant (about compound nucleus energy) for products at 40 MeV, whereas, in general, these decrease for products displaced far from beta-stability (i.e. neutron-rich products) with increasing bombarding energy. This is more evident for the 85 MeV data.

The overall trends in Figs. 10 and 11 indicate that the direct interaction is not as predominant at 40 and 55 MeV

FIGURE 10

Cascade deposition energy versus $Z_A - \langle Z \rangle$ of the observed fission products. The values of <Z> are taken from Table V, corresponding to those obtained from using UCD hypothesis.

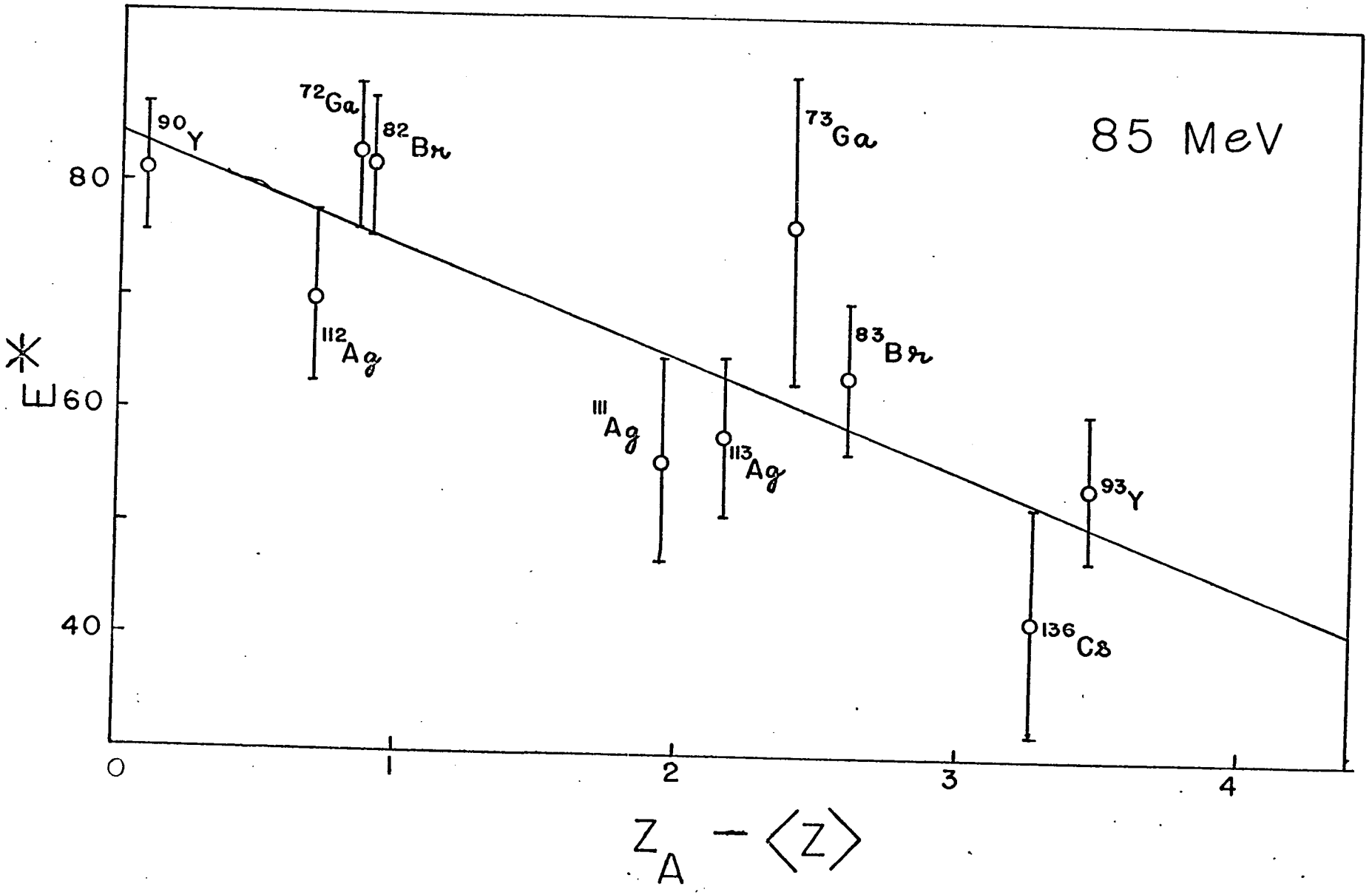
85 MeV
^{90}Y
^{72}Ga
^{82}Br
^{73}Ga
^{112}Ag
^{83}Br
^{111}Ag
^{113}Ag
^{93}Y
^{136}Cs
80
60
40
E*
0
1
2
3
4
$Z_A - \langle Z \rangle$

FIGURE 11

Cascade deposition energy versus $Z_A - \langle Z \rangle$ of the observed fission products. The values of $\langle Z \rangle$ are taken from Table V, corresponding to those obtained from using UCD hypothesis.

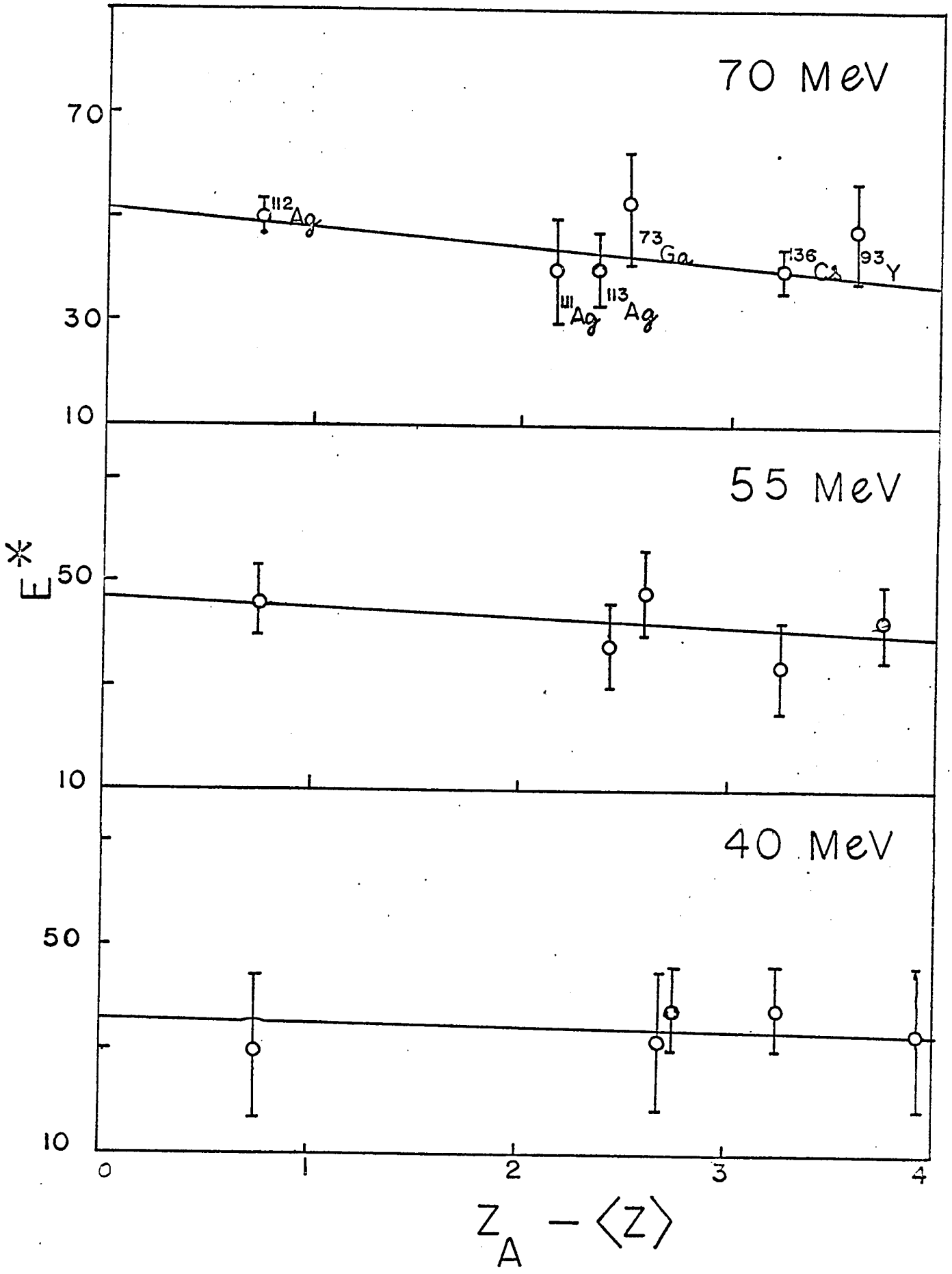
70 MeV
55 MeV
40 MeV
70
30
10
50
10
50
10
E^*
0
1
2
3
4
$Z_A - \langle Z \rangle$
^{112}Ag
^{111}Ag
^{113}Ag
^{73}Ga
^{136}Cs
^{93}Y

as it is at 70 and 85-MeV proton fission. The variation of the deposition energy with Z_A-<Z> of the products at different energies further indicates that a broader spectrum of deposition energies in the cascade nuclei is obtained with increasing bombarding energy. This is in line with the fact that at low energies a compound nucleus mechanism is valid leading to unique excitation energy and at higher energies the direct interaction predominates resulting in a broad distribution of deposition energies in the cascade residual nuclei.

It is apparent, particularly at 85-MeV, that the products of lower Z_A-<Z> are formed from higher deposition energy events and the reverse is true for neutron-excess products. This results from the fact that a larger amount of deposition energy in the cascade nuclei results in an increase in the excitation energy of the primary fragment. This highly excited primary fragment will emit relatively more neutrons thus leading to a rather neutron-deficient product. These conclusions were also made by Sugarman et al. (21) and Hogan and Sugarman (41) from the recoil study of ^{238}U fission induced by 450-MeV protons, and also by Noshkin and Sugihara (53) in the 150-MeV proton fission of ^{238}U.

It should be pointed out that the values of deposition energy and their interpretations are based on the cascade model of Chen et al. (12), and they may be significantly dif-

ferent if a different nuclear reaction model is used.

IV-4 Properties of Primary Fragments

The calculation of the kinetic and excitation energies of the primary fragments which lead to the experimentally measured fission products requires a knowledge of the average fissioning nucleus. The average charge and mass of the fissioning nucleus was obtained from the output of the cascade calculations of Chen et al. (12). A scrutiny of the output from the cascade calculation for 40, 55, 70, and 85-MeV proton bombardment of ^{238}U reveals that the average charges of the cascade nuclei are 92.9, 92.8, 92.7, and 92.7 respectively, and the average masses are 238.5, 238.4, 238.2, and 238. Despite small differences in charges and masses of the cascade nuclei at different bombarding energies, the average charge 93.0 and the average mass 238.0 of the cascade nuclei were used for all bombarding energies. Use of such a unique cascade nucleus $^{238}_{93}Np$, does not introduce serious error in the calculation of the kinetic energies of primary fragments. For 25-MeV bombardment, the compound nucleus $^{239}_{93}Np$ was used.

The following procedure was adopted to calculate the average fissioning nucleus. The compound nucleus or cascade nucleus was considered either to fission or to emit a neutron. The residual nucleus is further subjected to a competition between fission and neutron emission, depending

upon the excitation energy. The excitation energies of the successive fissioning nuclei were obtained by subtracting the binding energy B_n of the neutron plus the kinetic energy 2T (twice the nuclear temperature of the residual nucleus) from the excitation energies of the preceding fissioning nuclei. The nuclear temperature T, was calculated from (81)

$$E = aT^2 - 4T \qquad \text{(IV-11)}$$

where E is the excitation energy and a is the level density parameter, taken to be 10.5 MeV^{-1} (82). The values of B_n were taken from Myers and Swiatecki (83). The fission branching ratio G($G = \Gamma_f/(\Gamma_f + \Gamma_n)$ where Γ_n and Γ_f are the neutron emission width and fission width) for each fissioning nucleus in the fission chain was obtained from Huizenga and Vandenbosch (82). The mass and excitation energy of the average fissioning nucleus was then obtained by weighting the mass and excitation energy of each fissioning nucleus with its fission branching ratio. Since proton evaporation was considered negligible, the average charge of the fissioning nucleus remained unchanged i.e. 93.0. The values of the average mass $\langle A_f \rangle$ and excitation energy $\langle E_f^* \rangle$ of the fissioning nucleus are given in Table VII.

Each fissioning nucleus can lead to a number of primary fragments which in turn lead to the formation of the observed fission products. Corresponding to each of the fission products, 5 trial fragments whose mass numbers are higher by 5 or less mass units, were chosen. Since proton

evaporation was considered negligible, only neutron-excessive isotopes of the observed fragments were chosen.

The different properties of the primary fragments leading to the observed fission products were calculated according to the formalism given by Sugarman et al. (21). In all cases, the primary fragments are indicated by primed quantities, the observed fission products by unprimed quantities and the fissioning nucleus by the subscript f.

The following assumptions were made in the calculation of the different properties of the primary fragments.

(a) The kinetic energy of the primary fragment leading to the observed fission product is related to that of the observed product by

$$T(Z',A') = T(Z,A) \times \frac{A'}{A} \qquad \text{(IV-12)}$$

This relationship assumes that neutron evaporation does not change the velocity of the fragment and only reduces the kinetic energy of the fragment proportional to the reduction in its mass.

(b) The total kinetic energy T_o of the two fission fragments is shared between them in the inverse ratio of their masses, according to the conservation of momentum, so that

$$T_o = T(Z',A')\left[A_f/(A_f - A')\right] \qquad \text{(IV-13)}$$

(c) The total excitation energy of both primary fragments E^*_o is given by

$$E_o^* = \langle E_f^* \rangle + \Delta M(Z_f, A_f) - \Delta M_1(A_1', Z_1')$$

$$- \Delta M_2(A_2', Z_2') - T_o \qquad \text{(IV-14)}$$

Here $\Delta M(Z_f, A_f)$ is the ground-state mass excess of the fissioning nucleus. ΔM_1 and ΔM_2 are the mass excesses of complementary fragments, and the values were taken from Myers and Swiatecki (83). The total kinetic energy T_o was calculated from equation (IV-13).

(d) The primary fragments share the total excitation energy proportional to its mass i.e.

$$E^*(Z', A') = E_o^* \times \frac{A'}{A_f} \qquad \text{(IV-15)}$$

(e) All primary fragments were then considered for neutron evaporation assuming that each neutron carries away energy equal to the binding energy plus twice the nuclear temperature calculated with level density parameter a equal to A/20 (82). Proton evaporation was ignored because the measured products are mostly neutron-excessive. Only those fragments were chosen which could lead to the formation of the observed fission products. The selection of only these fragments may overestimate their contribution to the formation of the observed fission product, but this is probably cancelled by the underestimation of the rejected primary fragments which could partly lead to the formation of the products of interest.

The values of T and E* of the observed fission products were used to calculate T(Z',A') and E*(Z',A') for

the primary fragments. The primary mass number A' was determined for each independent or cumulative fission product. Hogan and Sugarman (41) calculated the kinetic energy and the excitation energy of each precursor of an observed cumulative fission product from the dependence of E* on $\langle N\rangle/\langle Z\rangle$ and T on $\frac{\langle N\rangle/\langle Z\rangle}{A}$ for the fission products. These values were then weighted by the fractional chain yield to calculate the grand average for an observed cumulative product. In our present work, we have used the kinetic energy and the excitation energy of the cumulative fission product as such, as has been done by Sugarman et al. (21). It can, however, be shown that the values of A' calculated for each member of a chain were the same within about one mass unit with the exception of the heaviest fission products, in spite of the large differences in the excitation energies. This results from the increase in neutron binding energy and the average neutron kinetic energy with increasing charge Z, which just about cancels out the increase in E* with increasing Z. The heaviest nuclide in the present work is ^{136}Cs which is a shielded nuclide. Therefore, the A' values calculated for cumulative products which are relatively lighter are rather unique mass numbers (i.e. rounded figures).

The results of these calculations are summarized in Table VII. Column 1 gives the observed product, column 2 the bombarding energy, column 3 the average charge of the fissioning nucleus, column 4 the mass of the average fissioning nucleus,

TABLE VII

Properties of Fissioning Nucleus and Primary Fragments

Nuclide	E_p MeV	<Z>	$\langle A_f \rangle$	A'	T(Z',A') MeV	E*(Z',A') MeV	T_o MeV	E^*_o MeV	$\langle E^*_f \rangle$ MeV
^{136}Cs	85	92.7	236.4	139	66.0	32.5	160.4	55.3	22.0
	70	92.7	236.5	139	67.0	29.7	162.0	50.6	21.6
	55	92.8	236.8	139	66.5	29.5	161.1	50.3	18.2
	40	92.9	236.8	139	66.9	29.1	162.1	49.6	18.5
	25	93.0	236.8	139	66.0	30.2	160.4	51.4	18.6
^{113}Ag	85	92.7	235.8	116	81.6	32.2	158.0	66.6	32.2
	70	92.7	236.0	116	80.2	29.0	155.8	61.8	26.4
^{112}Ag	85	92.7	235.4	115	81.1	36.4	158.6	74.6	35.0
	70	92.7	236.1	115	79.6	33.1	155.1	68.0	26.1
	55	92.8	236.3	115	80.2	31.7	156.3	65.1	24.4
	40	92.9	236.4	114	81.4	28.3	157.4	58.6	20.7
^{111}Ag	85	92.7	235.9	113	83.7	30.3	160.6	63.3	29.4
	70	92.7	236.4	113	82.6	28.3	158.2	59.2	22.1
	55	92.8	236.5	112	81.8	27.5	156.5	57.6	21.1
	40	92.9	236.8	112	80.1	27.8	153.3	58.2	18.6
	25	93.0	236.8	112	79.5	28.0	152.1	54.4	18.6
^{93}Y	85	92.7	235.8	95	96.5	24.5	161.6	60.9	31.3
	70	92.7	236.0	95	96.0	22.5	160.6	56.0	25.4
	55	92.8	236.5	95	94.9	21.9	158.6	54.6	22.0
	40	92.9	236.8	95	94.5	21.3	158.0	53.1	19.8
	25	93.0	236.8	95	93.1	22.9	156.8	51.2	18.6
^{90}Y	85	92.7	235.2	92	87.5	20.0	147.8	56.2	38.4
^{83}Br	85	92.7	235.6	85	94.5	24.9	147.9	68.9	32.3
^{82}Br	85	92.7	235.1	84	99.3	23.0	154.5	64.0	37.9
^{73}Ga	85	92.7	235.2	75	98.7	29.7	144.9	93.1	68.1
	70	92.7	236.1	75	98.5	24.2	144.3	76.2	51.7
	55	92.8	235.5	74	96.7	18.5	142.0	59.1	84.8
	40	92.9	236.1	74	95.6	17.1	140.0	54.7	18.6
	25	93.0	236.8	74	95.1	13.6	138.5	43.3	18.6
^{72}Ga	85	92.7	234.8	74	102.6	18.6	149	59.8	43.2

column 5 the mass of the primary fragment, columns 6 and 7, the kinetic and excitation energies of these fragments, and columns 8 and 9 the total kinetic and excitation energies of both fragments formed in fission. Column 10 lists the average excitation energy of all the fissioning nuclei leading to the observed fission fragment.

The errors in the calculation of the properties of individual primary fragments arise mainly from the assumptions made above. It is rather difficult to estimate the errors involved in these assumptions. Also the average quantities of the primary fragment should have been calculated for each progenitor of the cumulative fission products and weighted by its fractional chain yield. The selection of only one primary fragment for each fission product certainly over-emphasizes its contribution. However, as already mentioned, this is cancelled by the rejection of other fragments. Neglect of proton evaporation is prompted by the fact that the trial fragments are neutron-excessive. We estimate that the values of z', A', E*(Z',A'), T(Z',A'), E_o^* and T_o are correct to 0.2 charge unit, 1 mass unit, 3 MeV, 1 MeV, 4 MeV and 2 MeV respectively. Moreover, the Z_p values calculated from the UCD hypothesis may not be representative for the different chains encountered in the present work. If the observed product is far from the most probable charge, then the error introduced in average charge $\langle Z \rangle$ may be quite large. Unless Z_p is known experimentally, this error is very difficult

to estimate.

The total kinetic energy release T_o has been plotted against the mass ratio A'_H/A'_L of the primary fragments in Fig. 12. The mass of the complementary primary fragment was obtained by subtracting A' from $\langle A_f \rangle$ given in Table VII. These plots are given for different bombarding energies. The solid lines drawn through the points indicate that there is an amount of kinetic energy deficit at each bombarding energy. This 'kinetic energy deficit' has been defined as the difference between the maximum kinetic energy and that for symmetric fission. The most striking feature of Fig. 12 is that the 'kinetic energy deficit' decreases with increasing bombarding energy.

For comparison, we have tabulated all other pertinent data on kinetic energy deficit including the data from the present work in Table VIII. It is seen from this table that the trend of decrease in kinetic energy deficit with increasing bombarding energy is obvious in the energy range of thermal to 450 MeV. Sugarman et al. (21) have pointed out that the total kinetic energy of symmetric fission-fragments increases and that of asymmetric fission-fragments decreases with increasing bombarding energy. Consequently, there will be a decrease in "kinetic energy deficit' as the bombarding energy increases.

Now the question arises - why is there a 'kinetic energy deficit'? Britt et al. (84) have explained the varia-

FIGURE 12

Total kinetic energy between the fragment pair versus their mass ratio. Kinetic energy-deficit is obtained from this figure.

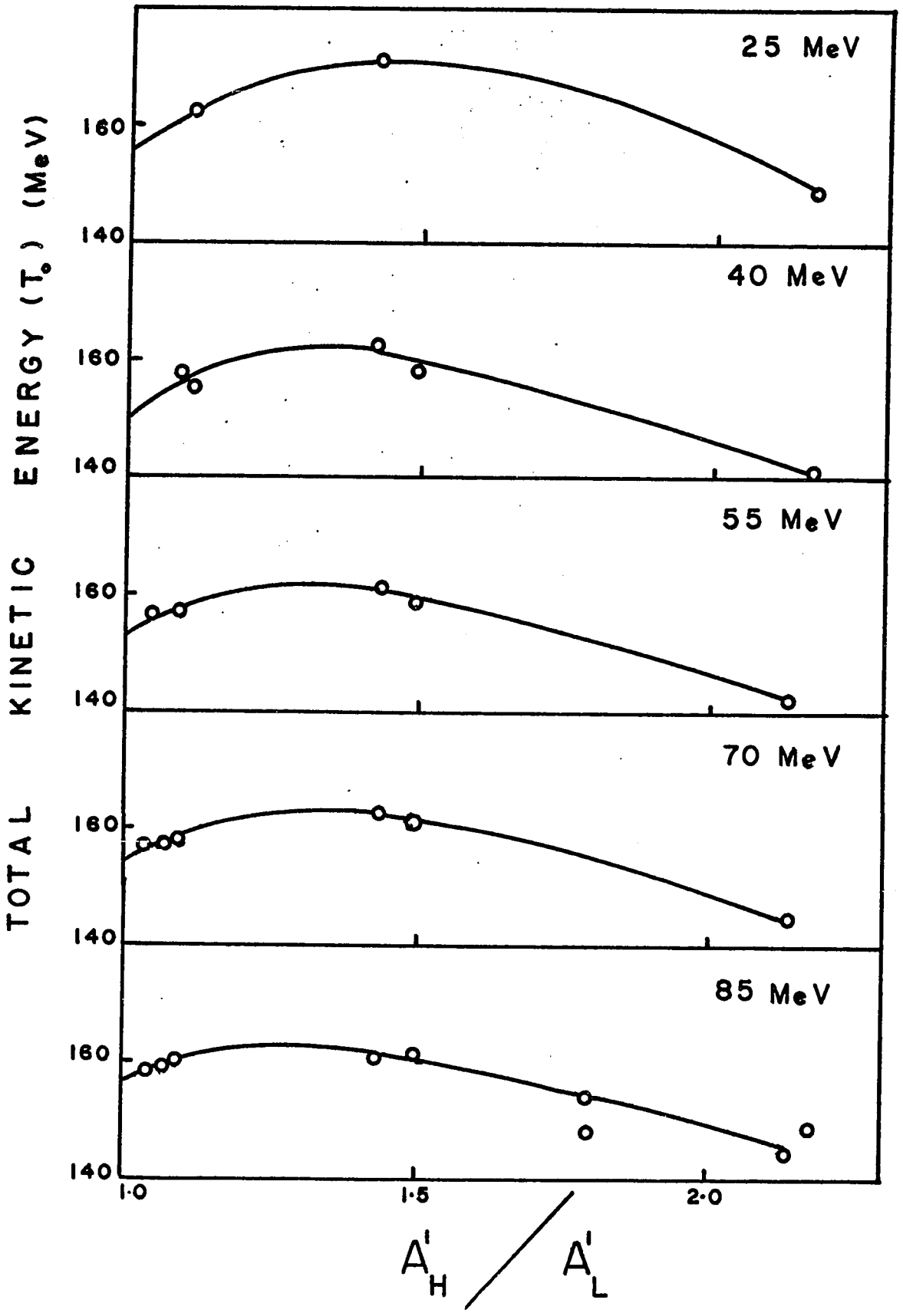
25 MeV
40 MeV
55 MeV
70 MeV
85 MeV
TOTAL KINETIC ENERGY (T_o) (MeV)
160
140
1·0
1·5
2·0
A'_H / A'_L

TABLE VIII

Kinetic Energy Deficit at Symmetric Fission

for Uranium Nuclides (21)

Target nuclide	Bombarding particle	Deficit (Mev)	Reference	Experimental technique
^{235}U	thermal n	40	(47)	Time of flight
		22	(86)	Solid state detector
		30	(51)	Solid state detector
		31	(31)	Recoil range
		19-27	(27)	Recoil range
		27	(21)	Recoil range
^{235}U	14-MeV n	15	(27)	Ionization chamber
^{238}U	23-MeV ^{2}H	<5-11	(27)	Recoil range
^{233}U	25.5-MeV ^{4}He	6	(84)	Solid state detector
	21.8-25.7 MeV ^{4}He	8	(88)	Time of flight
	29.7-MeV ^{4}He	6	(88)	Time of flight
^{238}U	29.7-MeV ^{4}He	7	(89)	Time of flight
	42.0-MeV ^{4}He	4		Solid state detector
^{238}U	450-MeV ^{1}H	2-5	(21)	Recoil range
		7-10		
^{238}U	25-85-MeV ^{1}H	16-6.5	Present study	Recoil range

tion of total kinetic energy, with fission fragment mass in terms of 'two-mode-hypothesis' of fission. According to this hypothesis there are two types of fission: (a) symmetric fission with highly excited fragments of low kinetic energy and (b) asymmetric fission with moderately excited fragments of high kinetic energy. These authors explained the lower kinetic energy release from symmetric fission by a greater distance between charge centres at the scission point for the symmetric mode than for the asymmetric mode.

Vandenbosch (85) has suggested that this 'kinetic energy deficit' arises from the nuclear shell structure of the fragments. If the fragments have a closed-shell structure, the deformation of these fragments will be very small. Vandenbosch (85) has shown that nuclei in the symmetric fission fragment region are found to be highly deformed, thus resulting in an elongated scission configuration. Thus the coulomb repulsion energy will be smaller for the symmetric fission mode than for the asymmetric fission mode.

In order to see this explanation more clearly, we have calculated the separation distance of the charged centres of two primary fragments at the scission point from the knowledge of the total kinetic energy T_o and the following relationship (21):

$$T_o = \frac{1.44\ Z(93 - Z)}{D} \qquad \text{(IV-16)}$$

where Z is the average charge of the primary fragment (see Table VII) and the values of D are given in Table IX along with mass ratio of the fragments. The values of D are plotted against A'_H/A'_L in Fig. 13. The values of D have an uncertainty of $\pm$ .4 fermis. It can be seen from Table IX and Fig. 13 that at any given bombarding energy the separation distance D is larger for symmetric fission products than for asymmetric ones, which confirms the above-mentioned explanation of the 'kinetic energy deficit'.

An examination of Table VII indicates that the total kinetic energy is rather insensitive to the bombarding energy even though the excitation energy involved in the fission does vary appreciably at different bombarding energies. This indicates that the average <D> (averaged over all mass-splits) is the same at all bombarding energies. We have calculated the average value of <D> by the algebraic average of the D values for all products at a given bombarding energy and they are tabulated in Table X along with other reported data.

The <D> values are constant within about 0.2 fermis in the energy range of 25-85 MeV. On the other hand, the <D> values in the energy range of 25-85 MeV are larger than the value given for 450-MeV fission of ^{238}U. It has been observed by Sugarman et al. (21) from a comparison of various data that <D> increases with increasing $<A_f>$. Thus the observed discrepancy between <D> for 25-85 MeV fission and that for 450-MeV fission may be due to a smaller mass number

FIGURE 13

Distance between the charge centres of the fragment pair versus the ratio of their masses.

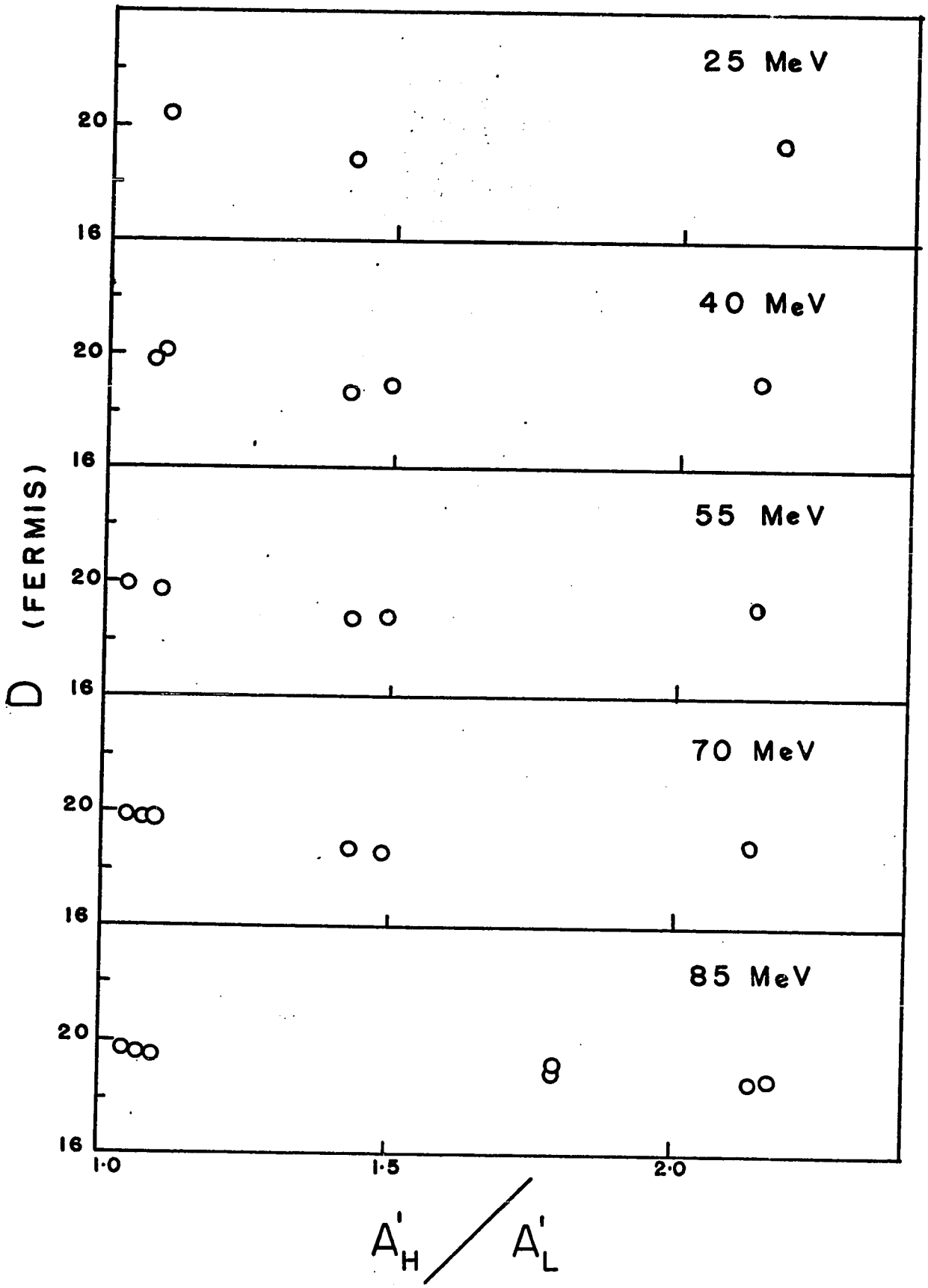
25 MeV
40 MeV
55 MeV
70 MeV
85 MeV
D (FERMIS)
20
16
1·0
1·5
2·0
A'H / A'L

TABLE IX

Values of D and the Mass-Ratios

Nuclide	E_p (MeV)	D (Fermis)	T_o (MeV)	A'_H/A'_L
^{136}Cs	85	18.8	160.4	1.43
	70	18.6	162.6	1.43
	55	18.7	161.1	1.43
	40	18.6	162.1	1.42
	25	18.8	160.4	1.42
^{113}Ag	85	19.6	158.0	1.03
	70	19.9	155.8	1.03
^{112}Ag	85	19.6	158.6	1.04
	70	19.8	157.1	1.04
	55	19.9	156.3	1.04
	40	19.8	157.4	1.08
^{111}Ag	85	19.4	160.6	1.09
	70	19.7	158.2	1.09
	55	19.8	156.5	1.10
	40	20.2	153.3	1.10
	25	20.4	152.1	1.10
^{93}Y	85	18.5	161.6	1.49
	70	18.6	160.6	1.49
	55	18.8	158.6	1.49
	40	18.8	158.0	1.49
	25	19.2	156.8	1.49
^{83}Br	85	19.1	147.9	1.79
^{82}Br	85	18.9	154.5	1.79
^{73}Ga	85	18.8	144.9	2.13
	70	18.9	144.3	2.13
	55	19.2	142.0	2.13
	40	19.2	140.0	2.13
	25	19.4	138.5	2.17
^{72}Ga	85	18.7	149.0	2.17

TABLE X

Comparison of <D> Values for Various Bombarding Energies (21)

Target nucleus	Bombarding particle	<D> (Fermis)
^{209}Bi	125-MeV ^{12}C	17.9 ± .1
^{238}U	450-MeV ^{1}H	18.4 ± .5
^{238}U(a)	85-MeV ^{1}H	19.1
	70-MeV ^{1}H	19.1
	55-MeV ^{1}H	19.3
	40-MeV ^{1}H	19.4
	25-MeV ^{1}H	19.4
^{232}Th-^{238}U	125-MeV ^{12}C 166-MeV ^{16}O	18.6 ± .3
^{238}U-^{240}Pu	125-MeV ^{12}C 166-MeV ^{16}O	19.4 ± .1

(a) Present study.

$\langle A_f \rangle$ of the fissioning nucleus for 450-MeV fission. The constancy of <D> indicates that the increase in deposition energy does not essentially affect the act of fission (i.e. coulomb repulsion) but rather appears as the excitation energy which is dissipated by the emission of neutrons either before or after fission.

Finally, the total kinetic energy at a given bombarding energy was calculated by averaging over the values given for all measured products.

$$\overline{T}_o = \frac{\sum_i \sigma_i (T_o)_i}{\sum_i \sigma_i} \qquad \text{(IV-17)}$$

where σ_i is the yield of i^{th} product. The values of σ_i have been taken from elsewhere (76,78). The values of $\overline{T}_o$ are 160.2, 162.0, 161.0, 162 and 160.4 at bombarding energies of 85, 70, 55, 40, and 25-MeV. These values are comparable with 163 $\pm$ 8 MeV quoted 450-MeV proton fission of ^{238}U (21), 161 MeV for 150-MeV proton fission of ^{238}U (35), and 167 $\pm$ 6 MeV for 90-MeV neutron fission of ^{238}U (90) and 168 MeV for thermal neutron fission of ^{235}U (47).

IV-5 Angular Distribution of the Fission Products

The anisotropy parameters b/a of different fission products corresponding to the angular distribution of the form $a + b\cos^2\theta$ are given in Table IV. A brief discussion of the observed anisotropy in the angular distribution will be given below.

It has been found from the study of low-energy fission (91) that the anisotropy of the fission products is dependent on the excitation energy of the fissioning nucleus and the mass of the fission product. The b/a values for several products (^{136}Cs, ^{112}Ag, ^{111}Ag, ^{93}Y, and ^{73}Ga) have been plotted against the average deposition energy E* in Fig. 14. This figure shows that there is no definite correlation of b/a with E* for ^{73}Ga, ^{93}Y, and ^{136}Cs. For the silver isotopes of mass number 111 and 112, the b/a values do not vary appreciably with E*. The overall trend observed in Fig. 14 can be explained in terms of the variation in orientation of the spin I of the fissioning nucleus.

It is known that the anisotropies of fission fragments arises from the preferred emission of fragments in a plane perpendicular to the direction of the angular momentum vectors. In the case of fission following compound nucleus formation, the angular momentum vectors will be preferentially oriented perpendicular to the beam direction and the angular distribution of the fragments will show peaks at 0° and 180°, thus leading to a positive anisotropy. Anisotropy is expected to increase with increasing excitation energy and angular momentum. At higher energy, direct interaction leads to transfer of relatively smaller amount of angular momentum. Moreover, the important factor in high-energy fission is the number of fissioning nuclei in the fission chain with broad distribution of excitation energy. The neutrons evaporated

FIGURE 14

Anisotropy parameter versus the deposition energy for various nuclides.

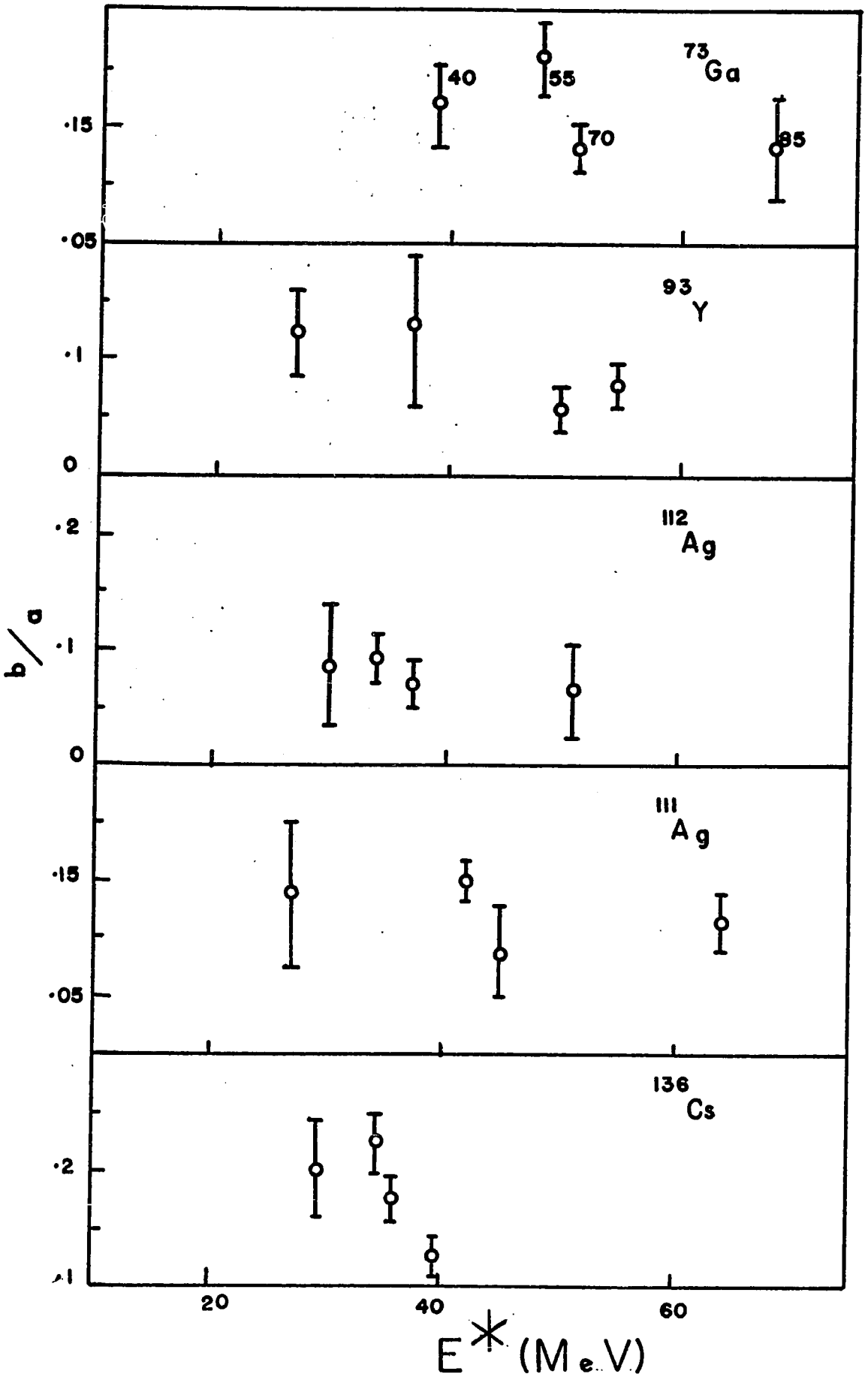
40
55
70
85
73 Ga
93 Y
112 Ag
111 Ag
136 Cs
.15
.05
.1
0
.2
.1
0
.15
.05
.2
.1
20
40
60
b/a
E* (MeV)

from each fissioning nucleus will carry away some angular momentum. Each of the fissioning nuclei will give rise to a specific anisotropy for a given product depending on the excitation energy and the angular momentum. The observed anisotropy may arise from all these factors.

Sugarman et al.(21) and Hogan and Sugarman (41) have shown, for ^{238}U fission with 450-MeV protons, that the values of b/a are negative for small values of E* ($\approx$-0.1 for E* $\approx$50 MeV) and positive for large deposition energies ($\approx$+0.1 for E*$\approx$200 MeV). Since all b/a values are positive in the present work, it is apparent that this correlation between b/a and E* observed at 450 MeV does not hold for the fission of ^{238}U by protons of energies 25-85 MeV. Crespo et al. (54) also did not find any correlation between b/a and E* in the proton fission of ^{238}U at 6.6 GeV.

In Fig. 15 we have plotted the b/a values for several products versus bombarding energy E_p. Meadows (92) found that the average anisotropy for gross fission products increases, passes through a maximum and then decreases with increasing bombarding energy. He observed a maximum for the b/a value at about 45 MeV. Sugarman et al. (21) also found a maximum of b/a at about 50 MeV for several fission products. Although the uncertainties are too large to tell whether maxima actually occur, the data for ^{136}Cs and ^{73}Ga are not inconsistent with maxima at about 40 and 55 MeV respectively. On the other hand, the b/a values for ^{111}Ag and ^{112}Ag are

FIGURE 15

Anisotropy parameter versus proton bombarding energy for the observed fission products.

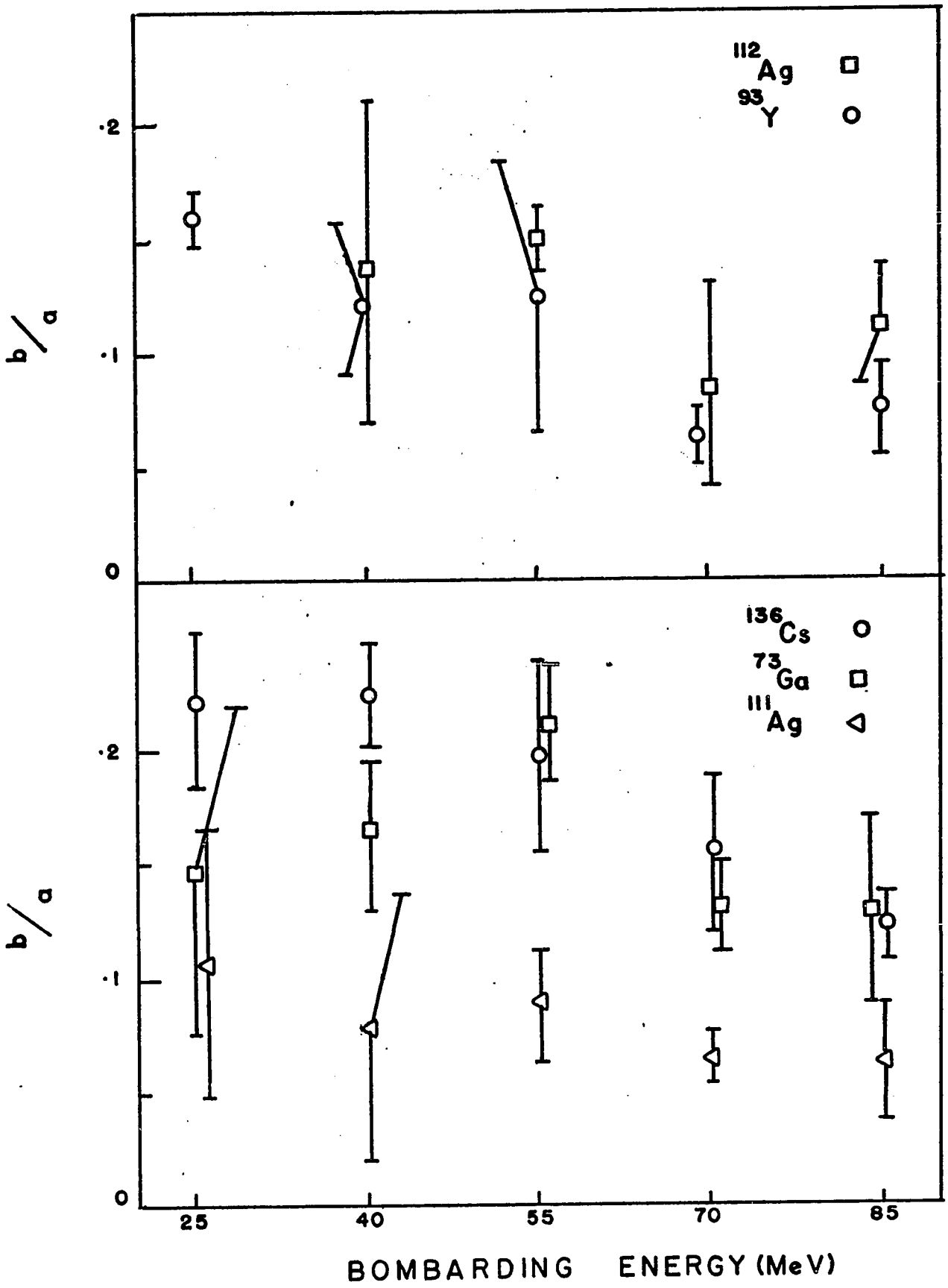
112Ag
93Y
136Cs
73Ga
111Ag
b/a
.2
.1
0
25
40
55
70
85
BOMBARDING ENERGY (MeV)

almost constant at all bombarding energies and those at ^{93}Y decrease with bombarding energy. The overall trend of these results can be explained by the complex phenomena associated with the cascade process. Halpern (91) predicted negative anisotropies for products formed from low-deposition energy cascade processes. He considered cascades involving low-deposition energies as arising from low-momentum transfer large-angle-collisions of the bombarding proton with nucleons inside the nucleus. These low-energy nucleons were assumed to deposit most of their kinetic energy and the angular momentum in the nucleus resulting in decreases values of b/a at higher energies. However, even the 85-MeV protons, the highest energy available in the present work are not large enough to make the anisotropy factor negative.

It has been shown by Cohen et al. (93,94) for 22-MeV proton fission of ^{238}U, ^{235}U, ^{233}U, ^{232}Th, and ^{230}Th that the anisotropy for asymmetric fission is larger than for symmetric fission. In order to see this effect, we have plotted the b/a values against the mass ratios of the fragments (taken from Table IV) in Fig. 16. While the b/a values increase rather slowly with increasing mass ratio at lower energies, the b/a values remain the same for all mass ratios at higher bombarding energies. At lower energies, a larger fraction of the reaction proceeds through compound nucleus formation and all products are formed from a fissioning nucleus having a rather unique excitation energy. Thus the

FIGURE 16

Anisotropy parameter versus mass ratio of the fission fragment pair.

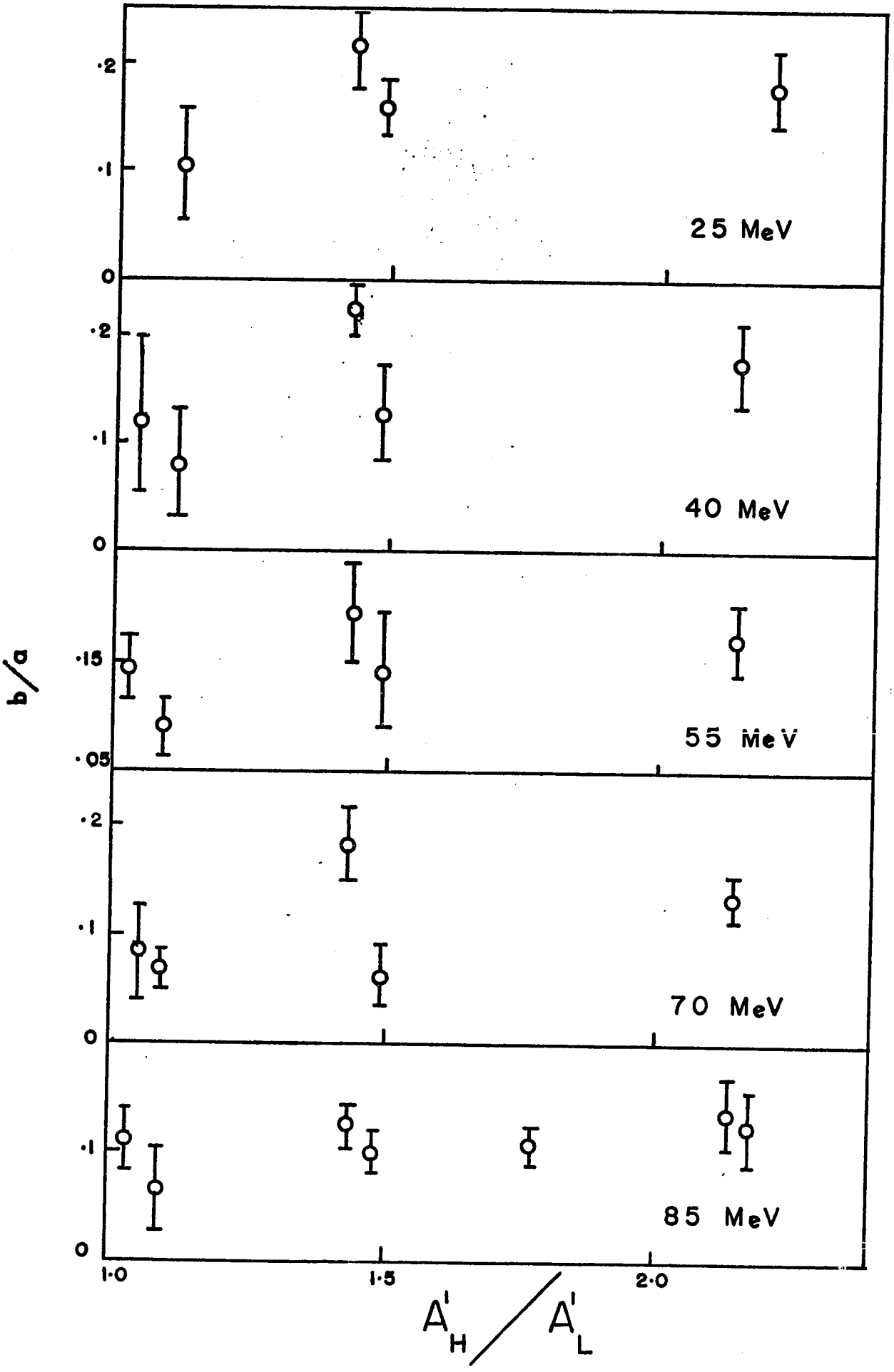
25 MeV
40 MeV
55 MeV
70 MeV
85 MeV
b/a
.2
.1
0
.15
.05
1·0
1·5
2·0
A'H / A'L

b/a values for symmetric and asymmetric fission modes could be differentiated. On the other hand, at higher energies the different products are produced from a variety of cascade nuclei with a wide distribution of excitation energy and, therefore, the anisotropies for all these products are probably averaged out to give the same values for both symmetric and asymmetric modes of fission.

V. SUMMARY AND CONTRIBUTION TO KNOWLEDGE

The recoil properties of ^{136}Cs, ^{113}Ag, ^{112}Ag, ^{111}Ag, ^{93}Y, ^{90}Y, ^{83}Br, ^{82}Br, ^{73}Ga, and ^{72}Ga produced in the fission of ^{238}U by protons of energies 25, 40, 55, 70, and 85 MeV have been measured radiochemically by the 'thick-target thick-catcher' method. The fractions of activities of each nuclide emitted in the forward, backward, and perpendicular directions relative to the proton beam were measured. These were then used to obtain the range R, the velocity parameter η, and the anisotropy parameter b/a.

The measured range R was converted to the kinetic energy for each product. The kinetic energy decreases, as expected, with increasing mass of the fission product.

The cascade deposition energy responsible for the formation of the measured product was derived from the experimentally measured $\eta_{||}$ and the relationship between the parallel component of linear momentum, $p_{||}$, and the deposition energy E*, obtained from Monte Carlo calculations. Also the perpendicular component $p_{\perp}$ of linear momentum was obtained for each product. It is found from the results that the neutron-deficient products are formed from cascade nuclei with high-deposition energy, whereas the converse is true for the neutron-excessive products. Furthermore, the results show that compound nucleus formation is the predominant mechanism

at lower energies and a direct interaction mechanism plays an increasingly greater role as the energy increases.

From the average deposition energy and the average cascade nuclei, the average fissioning nuclei and their average excitation energies were determined. The average kinetic energy and the excitation energy of the primary product fragment leading to each observed product has been determined. These were then used to calculate the total kinetic energy release corresponding to each product. The results indicate that there is a 'kinetic-energy deficit' in the symmetric mode of fission, compared to the asymmetric mode of fission. The 'kinetic-energy deficit' was, however, seen to decrease with increasing bombarding energy. The 'kinetic-energy deficit' was explained by the fact that the average distance of separation between the fragments in the symmetric mode of fission is larger than in the asymmetric mode of fission. This has been further corroborated by comparison with the average distance between the two charge centres, calculated from the observed total kinetic energy. These values were larger for symmetric fission than for asymmetric fission. The average total kinetic energy (averaged over all mass splits at a given bombarding energy) was found to be independent of bombarding energy indicating that increasing bombarding energy simply results in an increase in neutron emission and does not essentially affect the act of fission i.e. Coulomb repulsion. The average

distance <D> was found to be 19.3 + .2 fermi at all energies. The total kinetic energy release averaged over all products was 162 $\pm$ 4 MeV.

The anisotropy parameter b/a in the angular distribution of the fission products showed no definite correlation with E* and the values were all positive in the energy range of the present investigation. The dependence of anisotropy on bombarding energy showed maxima at 40 and 55 MeV for ^{136}Cs and ^{73}Ga respectively, whereas those for ^{111}Ag and ^{112}Ag remained almost constant at all bombarding energies. The b/a values for ^{93}Y decrease with increasing bombarding energy. These observations were explained in terms of complex phenomena associated with the cascade process. It was further noted that the b/a values were larger for asymmetric fission products than for symmetric fission products.

REFERENCES

1. O. Hahn and F. Strassmann, Naturwiss, 27, 11 (1939).

2. N. Bohr, Nature, 137, 344 (1936).

3. R. Serber, Phys. Rev., 72, 1114 (1947).

4. M.L. Goldberger, Phys. Rev., 74, 1268 (1948).

5. G. Bernardini, E.T. Booth, and S.J. Lindenbaum, Phys. Rev., 88, 1017 (1952).

6. H. McManus, W.T. Sharp, and H. Gellman, Phys. Rev., 93, A924 (1954).

7. G. Rudstam, 'Spallation of Medium Weight Elements', Ph.D. thesis, University of Uppsala, Sweden (1956).

8. N. Metropolis, R. Bivins, M. Storm, A. Turkevich, J.M. Miller, and G. Friedlander, Phys. Rev., 110, 185 (1958).

9. N. Metropolis, R. Bivins, M. Storm, A. Turkevich, J.M. Miller, and G. Friedlander, Phys. Rev., 110, 204 (1958).

10. F.P. Denisov, R.A. Latipova, V.P. Milovanov, and P.A. Cerenkov, J. Nucl. Phys., (U.S.S.R.), 1, 329 (1965).

11. H.W. Bertini, Phys. Rev., 131, 1801 (1963).

12. K. Chen, Z. Fraenkel, G. Friedlander, J.R. Grover, J.M. Miller, and Y. Shimamoto, Phys. Rev., 166, 949 (1968).

13. V.F. Weisskopf, Phys. Rev., 52, 295 (1937).

14. I. Dostrovsky, R. Bivins, and P. Rabinowitz, Phys. Rev., 111, 1659 (1958).

15. I. Dostrovsky, Z. Fraenkel, and G. Friedlander, Phys. Rev., 116, 683 (1959).

16. T. Ericson and V.M. Strutinski, Nucl. Phys., 8, 284 (1958).

17. T. Ericson and V.M. Strutinski, Nucl. Phys., 9, 689 (1959).

18. L. Winsberg and J.M. Alexander, Phys. Rev., 121, 518 (1961).

19. J.M. Alexander and L. Winsberg, Phys. Rev., 121, 529 (1961).

20. L. Winsberg, University of California Radiation Laboratory Report, UCRL-8618, 1959.

21. N. Sugarman, H. Munzel, J.A. Panontin, K. Wielgoz, M.V. Ramaniah, G. Lange, and E.L. Menchero, Phys. Rev., 143, 952 (1966).

22. J.A. Davies, J. Friesen, and J.D. McIntyre, Can. J. Chem., 38, 1526 (1960).

23. J.A. Davies, J.D. McIntyre, R.L. Cushing, and M. Lounsbury, Can. J. Chem., 38, 1535 (1960).

24. S. Katcoff, J.A. Miskel, and C.W. Stanley, Phys. Rev., 94, 128 (1954).

25. N. Bohr, Kgl. Danske Videnskab. Selskab, Mat.-Fys. Medd., 18, No. 8 (1948).

26. J.A. Panontin and N. Sugarman, J. Inorg. Nucl. Chem., 25, 1321 (1963).

27. J.M. Alexander, M.F. Gazdik, A.R. Trips, and S. Wasif, Phys. Rev., 129, 2659 (1963).

28. N. Bohr, Phys. Rev., 59, 270 (1941).

29. K.V. Marsh and J.A. Miskel, J. Inorg. Nucl. Chem., 21, 15 (1961).

30. F. Brown and B.H. Oliver, Can. J. Chem., 39, 616 (1961).

31. J.B. Niday, Phys. Rev., 121, 1471 (1961).

32. W.E. Stein, Phys. Rev., 108, 94 (1957).

33. N.O. Lassen, Proceedings of the International Conference on Peaceful Uses of Atomic Energy, Geneva, 1955, 2, 214 (1956).

34. J. Lindhard, M. Scharff, and H.E. Shiott, Kgl. Danske Videnskab. Selskab, Mat.-Fys. Medd., 33, No. 14 (1963).

35. V.E. Noshkin and T.T. Sugihara, J. Inorg. Nucl. Chem., 27, 943 (1965).

36. J.M. Alexander and M.F. Gazdik, Phys. Rev., 120, 874 (1960).

37. N.K. Aras, Ph.D. thesis, Massachusetts Institute of Technology (1964).

38. F. Suzor, Ann. Phys., 4, 269 (1949).

39. N. Sugarman, J. Chem. Phys., 15, 544 (1947).

40. B. Finkle, E.J. Hoagland, S. Katcoff, and N. Sugarman 'Radiochemical Studies': The Fission Products, C.D. Coryell and N. Sugarman, editors, National Nuclear Energy Series, McGraw-Hill Inc., Vol. 9, page 471 (1951).

41. J.J. Hogan and N. Sugarman (submitted to the Physical Review).

42. G.N. Walton, Prog. Nucl. Phys., 6, 192 (1957).

43. B.G. Harvey, Ann. Rev. Nucl. Sci., 10, 235 (1960).

44. J.M. Alexander, 'Nuclear Chemistry': Studies of Nuclear Reactions by Recoil Techniques, L. Yaffe, editor, Academic Press Inc., Vol. I, page 273 (1968).

45. N.T. Porile and N. Sugarman, Phys. Rev., 107, 1410 (1957).

46. W.E. Stein and S.L. Whetstone, Jr., Phys. Rev., 110, 476 (1958).

47. J.C.D. Milton and J.S. Fraser, Can. J. Phys., 40, 626 (1962).

48. J.M. Alexander, C. Baltzinger, and M.F. Gazdik, Phys. Rev., 129, 1826 (1963).

49. N.T. Porile, Phys. Rev., 120, 572 (1960).

50. N.K. Aras, M.P. Menon, and G.E. Gorden, Nucl. Phys., 69, 337 (1965).

51. W.M. Gibson, T.D. Thomas, and G.L. Miller, Phys. Rev. Lett., 7, 65 (1961).

52. S. Mukerji and L. Yaffe, Can. J. Chem., 43, 232 (1965).

53. V.E. Noshkin and T.T. Sugihara, J. Inorg. Nucl. Chem., 27, 959 (1965).

54. V.P. Crespo, J.B. Cumming, and A.M. Poskanzer, Phys. Rev., 174, 1455 (1968).

55. G.B. Saha and L. Yaffe, Can. J. Chem., 47, 655 (1969).

56. J.A. Panontin and N. Sugarman, J. Inorg. Nucl. Chem., 25, 1321 (1963).

57. N. Sugarman, M. Compos, and K. Wielgoz, Phys. Rev., 101, 388 (1956).

58. C.C. Casto, 'Analytical Chemistry of the Manhattan Project', NNES, Division VIII, Vol. 1, page 523 (1950).

59. J.A. Marinsky and E. Eichler, J. Inorg. Nucl. Chem., 12, 223 (1960).

60. L.E. Glendenin, R.R. Edwards, and H. Gest, 'Radiochemical Studies': The Fission Products (edited by C.D. Coryell and N. Sugarman), NNES, Plutonium project record, Vol. 9, page 1451, McGraw-Hill Inc., New York (1951).

61. G.E. Glendenin and R.P. Metcalf, ibid., page 1625 (1951).

62. C.W. Stanley, 'The Radiochemistry of the Rare Earths, Scandium, Yttrium, and Actinium' (edited by P.C. Stevenson and W.E. Nerwik), Subcommittee on Radiochemistry, NAS-NS 3020 (1961).

63. L.E. Glendenin, 'Radiochemical Studies': The Fission Products (edited by C.D. Coryell and N. Sugarman) NNES, Plutonium project record, Vol. 9, 1580, McGraw-Hill Inc., New York (1951).

64. H.B. Evans, ibid., page 1646 (1951).

65. L.E. Glendenin and C.M. Nelson, ibid., page 1642 (1951).

66. C.M. Lederer, J.M. Hollander, and I. Perlman, 'Table of Isotopes' Sixth edition, John Wiley and Sons Inc. (1967).

67. J.B. Cumming, 'Application of Computers to Nuclear and Radiochemistry', National Academy of Sciences, National Research Council, Nucl. Sci. Series, NAS-NS 3107, page 25 (1962).

68. N.T. Porile, Phys. Rev., 135, A1115 (1964).

69. A. Ewart, C. Valentine, and M. Blann, Nucl. Phys., 69, 625 (1965).

70. L. Winsberg, University of California Radiation Laboratory Report, UCRL-8618, (1959).

71. H. Nakahara, Ph.D. thesis, Massachusetts Institute of Technology (1966).

72. J.B. Cumming and V.P. Crespo, Phys. Rev., 161, 287 (1967).

73. A.C. Wahl, J. Inorg. Nucl. Chem., 6, 263 (1958).

74. A.C. Wahl, R.L. Ferguson, D.R. Nethaway, D.E. Troutner, and K. Wolfsberg, Phys. Rev., 126, 1112 (1962).

75. R.D. Evans, 'The Atomic Nucleus', McGraw-Hill Inc., New York, page 749 (1955).

76. J.H. Davies and L. Yaffe, Can. J. Phys., 41, 762 (1963).

77. S. Parikh, D.A. Marsden, N.T. Porile, and L. Yaffe, Can. J. Chem., 45, 1863 (1967).

78. A.H. Khan, Ph.D. thesis, McGill University (1968) (unpublished).

79. C.D. Coryell, M. Kaplan, and R.D. Fink, Can. J. Chem., 39, 646 (1961).

80. E.M. Douthett and D.M. Templeton, Phys. Rev., 94, 128 (1954).

81. H.K. Vonach, R. Vandenbosch, and J.R. Huizenga, Nucl. Phys., 60, 70 (1964).

82. J.R. Huizenga and R. Vandenbosch, Nuclear Reactions, Vol. II, edited by P.M. Endt and P.B. Smith, North-Holland Publishing Company, Amsterdam (1962).

83. W.D. Myers and W.J. Swiatecki, UCRL-11980 (1965) (unpublished).

84. H.C. Britt, H.E. Wegener, and J.C. Gwisky, Phys. Rev., 129, 2239 (1963).

85. R. Vandenbosch, Nucl. Phys., 46, 129 (1963).

86. H.W. Schmitt, J.H. Neiler, F.J. Walter, and A. Chetham-Strode, Phys. Rev. Lett., 9, 427 (1962).

87. V.M. Adamov, S.S. Kovalenko, and K.A. Petrzhak, English Translation, Soviet Phys., -JETP 15, 1024 (1962).

88. S.L. Whetstone, Jr., Phys. Rev., 133, B613 (1964).

89. J.P. Unik and J.R. Huizenga, Phys. Rev., 134, B90 (1964).

90. J. Jungerman and S.C. Wright, Phys. Rev., 76, 1112 (1949).

91. I. Halpern, Nucl. Phys., 11, 522 (1959).

92. J.W. Meadows, Phys. Rev., 110, 1109 (1958).

93. B.L. Cohen, W.H. Jones, G.H. McCormick, and B.L. Ferrell, Phys. Rev., 94, 625 (1954).

94. B.L. Cohen, B.L. Ferrell-Bryan, D.J. Coombe, and M.K. Mullings, Phys. Rev., 98, 685 (1955).